Agonist-dependent Single Channel Current and Gating in $\alpha_4\beta_2\delta$ and $\alpha_1\beta_2\gamma_{2S}$ GABA$_A$ Receptors

Angelo Keramidas and Neil L. Harrison

CV Starr Laboratory for Molecular Neuropharmacology, Department of Anesthesiology, Weill Medical College of Cornell University, New York, NY 10021

The family of γ-aminobutyric acid type A receptors (GABA$_A$Rs) mediates two types of inhibition in the mammalian brain. Phasic inhibition is mediated by synaptic GABA$_A$Rs that are mainly comprised of α_1, β_2, and γ_2 subunits, whereas tonic inhibition is mediated by extrasynaptic GABA$_A$Rs comprised of $\alpha_{4/6}$, β_2, and δ subunits. We investigated the activation properties of recombinant $\alpha_4\beta_2\delta$ and $\alpha_1\beta_2\gamma_{2S}$ GABA$_A$Rs in response to GABA and 4,5,6,7-tetrahydroisoxazolo[5,4-c]pyridin-3(2H)-one (THIP) using electrophysiological recordings from outside-out membrane patches. Rapid agonist application experiments indicated that THIP produced faster opening rates at $\alpha_4\beta_2\delta$ GABA$_A$Rs (β ∼1600 s^{-1}) than at $\alpha_1\beta_2\gamma_{2S}$ GABA$_A$Rs (β ∼ 460 s^{-1}), whereas GABA activated $\alpha_1\beta_2\gamma_{2S}$ GABA$_A$Rs more rapidly (β ∼1800 s^{-1}) than $\alpha_4\beta_2\delta$ GABA$_A$Rs (β < 440 s^{-1}). Single channel recordings of $\alpha_1\beta_2\gamma_{2S}$ and $\alpha_4\beta_2\delta$ GABA$_A$Rs showed that both channels open to a main conductance state of ∼25 pS at −70 mV when activated by GABA and low concentrations of THIP, whereas saturating concentrations of THIP elicited ∼36 pS openings at both channels. Saturating concentrations of GABA elicited brief (<10 ms) openings with low intraburst open probability (P$_O$ ∼ 0.3) at $\alpha_4\beta_2\delta$ GABA$_A$Rs and at least two "modes" of single channel bursting activity, lasting ∼100 ms at $\alpha_1\beta_2\gamma_{2S}$ GABA$_A$Rs. The most prevalent bursting mode had a P$_O$ of ∼0.7 and was described by a reaction scheme with three open and three shut states, whereas the "high" P$_O$ mode (∼0.9) was characterized by two shut and three open states. Single channel activity elicited by THIP in $\alpha_4\beta_2\delta$ and $\alpha_1\beta_2\gamma_{2S}$ GABA$_A$Rs occurred as a single population of bursts (P$_O$ ∼0.4–0.5) of moderate duration (∼33 ms) that could be described by schemes containing two shut and two open states for both GABA$_A$Rs. Our data identify kinetic properties that are receptor-subtype specific and others that are agonist specific, including unitary conductance.

INTRODUCTION

The γ-aminobutyric acid type A receptor (GABA$_A$R) is a member of the Cys-loop superfamily of ligand-gated ion channels (LGICs), and the main inhibitory receptor in the brain. GABA$_A$Rs are comprised of five homologous subunits that assemble to form a central, Cl$^-$-selective pore. Cloning techniques have so far identified 16 subunits that occur in mammals, these include $\alpha_{1–6}$, $\beta_{1–3}$, $\gamma_{1–3}$, δ, ε, π, and θ subunits (Sieghart and Sperk, 2002; Darlison et al., 2005).

At inhibitory synapses the most prevalent GABA$_A$R is composed of α_1, β_2, and γ_2 subunits (McKernan and Whiting, 1996; Somogyi et al., 1996), which has been shown by covalent subunit cross-linking experiments to have a stoichiometry and arrangement of $\gamma_2\beta_2\alpha_1\beta_2\alpha_1$ (Chang et al., 1996; Baumann et al., 2002). This type of GABA$_A$R can be found, for example, at synapses in the cerebellum (Vicini et al., 2001). GABA release at these fast inhibitory synapses is brief and results in a submillisecond, high concentration pulse of GABA, and this elicits a phasic or transient response that typically lasts <50 ms (Cobb et al., 1995; Hardie and Pearce, 2006). The inhibitory synaptic currents can be modeled mathematically using a pulse of ∼1 mM GABA for 300–500 μs (Jones and Westbrook, 1995; Lavoie et al., 1997; Schofield and Huguenard, 2007). The duration of the synaptic event is dependent on a variety of factors, of which one of the most important is the identity of the α subunit, with α_1 subunits mediating rapid decay kinetics (Vicini et al., 2001), whereas α_2 and α_3 subunits mediate slower events (Gingrich et al., 1995; Lavoie et al., 1997; Schofield and Huguenard, 2007).

In addition to the activation of conventional synaptic GABA$_A$Rs by neurotransmitter release, a form of tonic inhibition occurs due to the sustained activation of GABA$_A$Rs located extrasynaptically. These receptors are thought to be activated by low concentrations of agonists present in the extracellular space, such as GABA, as has been shown in the cerebellum (Brickley et al., 1996) and dentate gyrus (Mody, 2001), and taurine, as has been reported in the thalamus (Jia et al., 2008). Extrasynaptic GABA$_A$Rs are believed to be composed of α_4, $\beta_{2/3}$, and δ subunits in the thalamus, dentate gyrus, and cortex (Sur et al., 1999; Sieghart and Sperk, 2002; Jia et al., 2005), with α_6 subunits replacing α_4 subunits in the cerebellum.

Correspondence to Angelo Keramidas: ank2013@cornell.med.edu

The online version of this article contains supplemental material.

Abbreviations used in this paper: GABA$_A$R, γ-aminobutyric acid type A receptor; LGIC, ligand-gated ion channel; RI, rectification index; THIP, 4,5,6,7-tetrahydroisoxazolo[5,4-c]pyridin-3(2H)-one.

As the δ and γ subunits have not been shown to coexist in the same pentamers, it is widely presumed that the δ subunit simply replaces the γ to give an arrangement of δβαβα in αβδ GABA$_A$Rs (Sigel et al., 2006). In rat thalamus, 60–70% of the α$_4$ subunit protein coprecipitates with the δ subunit, which is thought to be exclusively extrasynaptic (Nusser et al., 1998), and all of the δ subunit is restricted to α$_4$ subunit–containing receptors (Sur et al., 1999). The α$_4$ and δ subunits confer pharmacological properties that differ from those of α$_1$β$_2$γ$_{2S}$ GABA$_A$Rs. GABA$_A$Rs containing the α$_4$ subunit are insensitive to conventional benzodiazepines (Knoflach et al., 1996; Whittemore et al., 1996) and show robust potentiation of GABA responses by neurosteroids (Whittemore et al., 1996). Concentration–response experiments on recombinant α$_4$β$_{2/3}$δ GABA$_A$Rs have demonstrated that these channels are activated with greater relative efficacy by the GABA analogue and hypnotic, 4,5,6,7-tetrahydroisoxazolo[5,4-c]pyridin-3(2H)-one (THIP; Gaboxadol) than GABA (Brown and Kerby, 2002; Jia et al., 2005), whereas the reverse applies to synaptic GABA$_A$Rs.

In this study we used rapid agonist application techniques in conjunction with single channel recordings to develop kinetic schemes for recombinant α$_4$β$_2$δ and α$_1$β$_2$γ$_{2S}$ GABA$_A$Rs, activated by GABA and THIP. Simple activation schemes derived from modeling fast agonist application experiments showed that THIP produces a greater opening rate constant at α$_4$β$_2$δ GABA$_A$Rs than GABA, whereas the converse was the case for α$_1$β$_2$γ$_{2S}$ GABA$_A$Rs. Saturating concentrations of THIP also evoked single channel openings with a larger conductance (∼36 pS) at both α$_4$β$_2$δ and α$_1$β$_2$γ$_{2S}$ GABA$_A$Rs, whereas low concentrations of THIP and high and low concentrations of GABA elicited openings that were ∼25 pS at both channels. Kinetic analysis of single channel recordings obtained from α$_4$β$_2$δ and α$_1$β$_2$γ$_{2S}$ GABA$_A$Rs corroborated the data from macropatch, ensemble experiments and revealed that channel bursting characteristics are both receptor and agonist specific. GABA induced up to three distinct modes in α$_1$β$_2$γ$_{2S}$ GABA$_A$Rs, identified by stable intraburst open probabilities; the mode with the highest intraburst open probability could be described by three open and two shut states. In contrast, only one gating mode was seen in α$_4$β$_2$δ GABA$_A$Rs, and the openings were brief. THIP elicited homogeneous bursting patterns in both channels, which consisted of brief bursts that could best be described by two open and two shut states.

MATERIALS AND METHODS

Expression of GABA$_A$Rs in HEK293 Cells
HEK293 cells were plated onto poly-D-lysine–coated glass coverslips and transfected with cDNA encoding the human α$_1$, mouse α$_4$, rat β$_2$, human γ$_{2S}$, and human δ subunits, using the calcium phosphate coprecipitation method. Mouse and rat subunits were combined with human subunits, first because of their availability,

and second, because they show a high degree of identity and homology with their human counterparts. The cells were also transfected with the CD4 surface antigen, which acted as a transfection marker. Our preliminary cotransfections of α$_4$, β$_2$, and δ subunits were done at a transfection ratio of 1:1:2 (plasmid mass ratio), but we settled on a ratio of 1:1:5 for the present study as our data suggested that that ratio favored the inclusion of the δ subunit to produce ternary α$_4$β$_2$δ GABA$_A$Rs. We also cotransfected the α$_4$ and β$_2$ subunits at a ratio of 1:1. α$_1$, β$_2$, and γ$_{2S}$ subunits were cotransfected at a ratio of 1:1:4. In addition, we mock transfected cells to test for the presence of endogenous THIP or GABA-gated currents. Transfected cells were washed after 24 h of exposure to the cDNA precipitate and used for patch-clamp recordings 48–72 h later.

Electrophysiology and Solutions
GABA and THIP-gated currents were recorded at room temperature (21 ± 1°C) using the excised outside-out patch configuration of the patch-clamp technique (Hamill et al., 1981). For a small number of experiments, whole-cell recordings were done as described in the results. Patches (and cells) were voltage clamped at −70 mV. Macropatch (ensemble) and single channel currents were recorded using an Axopatch-200A amplifier (Axon Instruments), filtered with a 4-pole Bessel filter that is built into the amplifier at a −3 dB value of 5 kHz (macropatch) or 10 kHz (single channels) and acquired at a sampling frequency of 20 or 50 kHz, respectively. The standard extracellular solution contained (in mM) 140 NaCl, 5 KCl, 2 CaCl$_2$, 1 MgCl$_2$, 10 D-glucose, and 10 HEPES, and titrated to a pH of 7.4 with NaOH. The standard intracellular solution contained (in mM) 60 NaCl, 60 CsCl, 3 KCl, 2 K$_2$ATP, 4 MgCl$_2$, 1 CaCl$_2$, 5 EGTA, 10 D-glucose, 10 HEPES, 20 TEACl, and pH adjusted to 7.4 with NaOH. The patch pipettes used for macropatch experiments had resistances of 4–7 MΩ when filled with intracellular solution. GABA and THIP were dissolved at the desired concentrations in the extracellular solution. Solutions were delivered onto the patches via a double lumen glass tube, mounted on a piezoelectric transducer that was controlled by programmed, pClamp software. The time taken for the small solution interface (∼5 nm) between the adjacent streams to sweep across the patch was ∼100–150 μs (rising phase of open pipette response). Recorded patches were positioned adjacent to the solution interface to achieve fast and consistent solution exchange. Multiple (2–10) currents were recorded at each agonist concentration and averaged to produce a net current response for analysis. Patch pipettes used for single channel recordings were made of thick walled borosilicate glass and had resistances of 6–15 MΩ when filled with intracellular solution. They were also coated with a silicon polymer (Sylgard 184) and fire polished to improve signal resolution. Recordings were made in the continuous presence of agonist. Saturating concentrations of THIP and GABA (10 mM) were used to determine the activation steps and associated rate constants for derived kinetic schemes.

Data Analysis
To determine the activation rate constant in macropatch recordings, the onset phase of the current response was fitted to the following exponential equation:
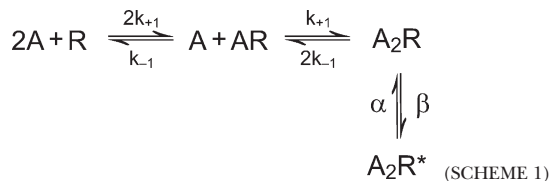
$$I(t) = I_{max}\left(1 - e^{-k_{obs}t}\right), \qquad (1)$$

where, $I(t)$ is the current at time t, I_{max} is the maximum current amplitude, and k_{obs} is the observed pseudo-first order rate constant for current activation. The activation rate constant (k_{obs}) was plotted against agonist concentration ($\log_{10}$ scale) for a range of concentrations and the data were fitted to a modified form of the Hill equation:

$$k_{obs} = \frac{k_{obs}^{max}[A]^n}{\left([A]^n + EC_{50}^{\ n}\right)} + y_O, \qquad (2)$$

where, $[A]$ is the agonist concentration, EC_{50} is the concentration of agonist that produces half of the maximal response, n is the Hill coefficient (slope at EC_{50}), k^{max}_{obs} is the maximal k_{obs}, and y_O is the lower activation rate constant as $[A]$ approaches zero. From the fitted data we extracted the maximum (upper asymptote) and minimum (lower asymptote) rates of activation and the concentration that elicits the half-maximal k_{obs} ($k_{obs}\, EC_{50}$).

We related our macropatch activation data to a modified del Castillo-Katz type scheme (Del Castillo and Katz, 1957) and assumed that the channels open from a diliganded state to single open state. Moreover, we treated the two putative agonist binding sites on each $GABA_A R$ as being identical and independent, so that the binding of one GABA molecule to its site does not affect the binding of the second GABA molecule:

$$2A + R \underset{k_{-1}}{\overset{2k_{+1}}{\rightleftharpoons}} A + AR \underset{2k_{-1}}{\overset{k_{+1}}{\rightleftharpoons}} A_2R$$

$$A_2R \underset{\beta}{\overset{\alpha}{\rightleftharpoons}}$$

$$A_2R^* \quad \text{(SCHEME 1)}$$

Where R represents the receptor, A represents the agonist, AR and A_2R are the mono- and diliganded receptor in the closed state, respectively, and A_2R^* is the diliganded receptor in the open state. k_{+1} and k_{-1} are the microscopic association and dissociation rate constants, respectively. β is the channel opening rate constant and α is the shutting rate constant. We interpreted the difference between the upper and lower asymptote values in the k_{obs} versus [agonist] plots as the opening rate constant in Scheme 1. The minimum rate of activation (lower asymptote) was taken as an estimate of the mean burst duration of the channels at low agonist concentration. In addition, reasonable estimates of agonist apparent affinity were obtained from the $k_{obs}\, EC_{50}$ values, after correcting for the independent binding site assumption (Maconochie and Steinbach, 1998; Keramidas et al., 2006). Estimates of the individual channel shutting, agonist binding, and unbinding rate constants were obtained by simulating macropatch currents in response to 1–2-ms exposure to agonist. Rapid application currents were simulated in conjunction with coupled differential equations that described the transitions between states. The simulations were done with Berkeley Madonna software (www.berkeleymadonna.com). Experimentally determined values, such as the opening rate constant and apparent affinity, were entered as fixed parameters in the simulations, whereas unknown rate constants, such as the shutting rate constant and the individual agonist binding and unbinding rate constants, were allowed to vary during the fitting.

Single channel current amplitude was determined by generating amplitude histograms for selected segments of record. Single channel conductance was calculated using the following expression:

$$\gamma = \frac{i}{(V_m - V_{rev})}, \tag{3}$$

where γ is the single channel conductance, i is the single channel current, V_m is the transmembrane potential and V_{rev} is the potential at which current reverses direction. The values of V_{rev} were obtained from current–voltage measurements, covering a range of voltages between −60 mV to +60 mV (Keramidas et al., 2002). Liquid junction potential offsets were calculated and accounted for in the conductance calculation (Barry, 1994).

For single channel analysis, we opted to focus on the gating steps of fully (di-) liganded channels in our kinetic modeling. We used saturating concentrations of agonist to isolate the gating steps from agonist binding. By activating the channels with saturating concentrations of agonist, any agonist binding steps rapidly

preequilibrate and the resulting activity can be safely assumed to arise from fully liganded channels. We also found that only saturating concentrations of THIP produces groups of openings that could be defined as clusters or bursts, especially at $\alpha_4\beta_2\delta$ channels. Subsaturating concentrations of THIP (e.g., 50 μM), mostly produced isolated openings at $\alpha_4\beta_2\delta$ channels, which precluded any useful analysis. Single channel kinetic analysis was done with the aid of QuB software (www.qub.buffalo.edu). Segments of activity that appeared to be due to multiple, overlapping openings (e.g., see Fig. 1 A and Fig. 4 A and Figs. S1 and S2) were excluded from analysis. Single channel currents were divided into segments or clusters of activity, initially by eye (see Fig. 4, C and D), and extracted to separate files within QuB for further analysis. Eye-selected clusters were separated from each other by quiescent periods lasting at least 100 ms (often much longer). Isolated openings that often occurred between clusters were ignored during cluster selection and not included in any subsequent analysis. Clusters were separated into discrete bursts by applying a critical shut time (t_{crit}) that marked the end of a burst (Colquhoun and Hawkes, 1995; Purohit and Grosman, 2006). t_{crit} values were determined of each patch by generating shut time histograms (MIL in QuB) for the idealized (SKM in QuB) eye-selected clusters of data (Lema and Auerbach, 2006; Plested et al., 2007). These preliminary fits, which were not used for further analysis or model derivation, were needed solely to determine t_{crit} values for the purpose of dividing eye-selected clusters into shorter segments of activity. The t_{crit} values were calculated by equalizing the area under the overlapping tails of the two longest shut distributions within eye-selected clusters. Clusters were divided into bursts because the longest shut "intracluster" duration generally ranged between 10 and 40 ms, making it possible that some clusters of openings arose from more than one channel, especially in patches where there was some evidence of more than one channel in the patch. To minimize the occurrence of this confound we opted to divide our clusters into burst, which increased the likelihood that the activity subjected to analysis arose from a single ion channel. The system dead time was 75 μs. Bursts were analyzed for duration, open probability (intraburst P_O), and open and shut durations. Gating schemes were derived by generating shut and open dwell-time histograms to idealized burst of data by the method of maximum likelihood (MIL "Star" within QuB) and fitting mixtures of probability density functions to these histograms (Colquhoun and Hawkes, 1995; Lema and Auerbach, 2006). The number of individual exponential components in each dwell class (shut or open) resulting from the fit was taken as the minimum number of states in any underlying reaction scheme. Postulated schemes were then refitted to the idealized bursts by maximum likelihood, starting with initial rate constants of 250 s^{-1}. Three criteria were used to rank schemes. First, the group of likelihood (log likelihood, LL) values obtained from three to five patches, for a particular experimental condition, was subjected to t test analysis. Second, we favored schemes that produced opening rate constants that were comparable to those obtained from macropatch experiments and, finally, schemes that reasonably simulated the macropatch data. Clusters of activity were separated into distinct modes based on intracluster open probability (P_O), using the "Select" option in QuB.

Online Supplemental Material

This paper contains two supplemental figures, Figs. S1 and S2 (available at http://www.jgp.org/cgi/content/full/jgp.200709871/DC1). Fig. S1 shows single channel recordings of agonist competition experiments in $\alpha_1\beta_2\gamma_{2S}$ GABA$_A$Rs using high and low concentrations of THIP (5 mM and 100 μM) and GABA (5 mM and 50 μM). Fig. S2 shows single channel recordings in $\alpha_1\beta_2\gamma_{2S}$ GABA$_A$Rs at high and low concentrations of THIP (5 mM and 100 μM) and GABA (5 mM and 50 μM) at pipette potentials of −70 and +70 mV.

RESULTS

Identifying the $\alpha_4\beta_2\delta$ Pentameric GABA$_A$R Using THIP

We recorded single channel currents in excised, outside-out membrane patches from cells transfected with α_4, β_2, and δ subunits, initially at a transfection ratio of 1:1:2. These patches exhibited two current amplitudes in response to saturating concentrations of THIP (10 mM), at a pipette potential of -70 mV. The most frequently observed openings had an amplitude of ~-2 pA, but we also observed ~-2.5 pA openings that were less frequent. These two current amplitudes could conceivably represent subconductance states of $\alpha_4\beta_2\delta$ GABA$_A$Rs having the conventionally accepted stoichiometry of $2\alpha_4{:}2\beta_2{:}\delta$ (Sigel et al., 2006). However, we decided to transfect cells at other transfection ratios and subunit combinations to investigate the possibility that the observed heterogeneity in single channel amplitude arose from GABA$_A$Rs of different composition. We first increased the proportion of δ subunit in our transfections to give a $\alpha_4{:}\beta_2{:}\delta$ ratio of 1:1:5. These transfections yielded a predominant single channel, THIP-activated current amplitude of -2.46 ± 0.07 pA ($n = 11$ patches). An example of this activity is shown in Fig. 1 A along with the pooled amplitude histogram (Fig. 1 B, dark gray shade). In our next set of transfections we omitted the δ subunit and cotransfected only the α_4 and β_2 subunits, at a ratio of 1:1. Fig. 1 A shows a typical example of single channel, THIP-activated currents from these transfections. The pooled amplitude histogram yielded a mean single channel current amplitude, calculated from 16 patches, of -1.96 ± 0.05 pA (Fig. 1 B, light gray shade). Similar experiments on patches excised from mock-transfected cells yielded no endogenous THIP (or GABA)-gated activity.

Our single channel measurements suggest that transfecting α_4, β_2, and δ subunits at a ratio of 1:1:2 likely results in the expression of GABA$_A$Rs of different subunit compositions, including not only the desired ternary $\alpha_4\beta_2\delta$ GABA$_A$Rs, but possibly binary $\alpha_4\beta_2$ channels. This inference is supported by our pooled amplitude histograms and statistical treatment of data obtained at different subunit transfection ratios. We performed a t test (unpaired) on the measurements of single channel current amplitude between the two groups of transfections (α_4 and β_2 at 1:1 and α_4, β_2, and δ at 1:1:5). This analysis produced a significant difference in current amplitude between the two groups, with a P value of <0.0001, suggesting that the latter transfection ratio results in the expression of a channel that opens to a distinct amplitude. We infer that this channel is likely the ternary $\alpha_4\beta_2\delta$ GABA$_A$R.

For subsequent sections of this study, including macropatch measurements, we transfected α_4, β_2, and δ subunits at a 1:1:5 ratio, as our data suggest that this ratio favorably biases the expression of ternary $\alpha_4\beta_2\delta$ GABA$_A$Rs. Moreover, in our single channel analysis we will disregard

the ~-2 pA currents in the same transfections as we cannot rule out the possibility that these openings are due to $\alpha_4\beta_2$ binary GABA$_A$Rs.

Single Channel Amplitude in $\alpha_4\beta_2\delta$ and $\alpha_1\beta_2\gamma_{2S}$ GABA$_A$Rs Is Agonist Dependent

In this set of experiments we measured and compared single channel current amplitude (and conductance) in $\alpha_4\beta_2\delta$ and $\alpha_1\beta_2\gamma_{2S}$ GABA$_A$Rs in response to GABA and THIP at a pipette potential of -70 mV. Saturating concentrations of GABA usually failed to evoke any currents in $\alpha_4\beta_2\delta$ GABA$_A$Rs in most patches that exhibited THIP-activated currents. Generally, the single channel openings in $\alpha_4\beta_2\delta$ GABA$_A$Rs that were observed in response to GABA were very short in duration, consisted mostly of single open–shut events, and disappeared within a few seconds of recording. GABA-gated single channel activity of $\alpha_4\beta_2\delta$ GABA$_A$Rs has been previously reported (Akk et al., 2004). That study also noted the absence of discrete clusters of openings, even though saturating concentrations (1 mM) of GABA were used. A notable feature of the GABA-gated currents that we observed was that they had a smaller current amplitude than when activated by THIP. As shown in Fig. 1 C and the accompanying pooled amplitude histogram in Fig. 1 D, GABA produced a single channel amplitude of -1.72 ± 0.07 pA ($n = 3$ patches). An unpaired, two-tailed t test revealed that the THIP-activated current amplitude was significantly greater than GABA-gated current (P < 0.0001).

We also examined single channel activity in cells transfected with α_1, β_2, and γ_{2S} subunits, at a ratio of 1:1:4 in response to THIP. These patches yielded a single current amplitude of -2.58 ± 0.08 pA ($n = 10$ patches; Fig. 1 E) at a pipette potential of -70 mV. In contrast, when we exposed $\alpha_1\beta_2\gamma_{2S}$ GABA$_A$Rs to GABA we observed single channel currents of two distinct amplitudes. One of these was ~-1.1 pA (unpublished data), but this was relatively rare, accounting for $\sim30\%$ of openings in only 3 out of 14 patches exposed to 10 mM GABA. The majority of the activity had an amplitude of -1.68 ± 0.06 pA ($n = 9$ patches; Fig. 1 E) and occurred in clusters, separated by quiescent periods that generally lasted several seconds (see also Fig. 4 C). This GABA-gated activity was similar to that previously reported for $\alpha_1\beta_1\gamma_{2S}$ channels (Lema and Auerbach, 2006) and the closely related $\alpha_1\beta_2\gamma_{2L}$ channels (Steinbach and Akk, 2001), also expressed in HEK293 cells. Fig. 1 F shows pooled amplitude histograms for THIP and GABA-gated single channel currents in $\alpha_1\beta_2\gamma_{2S}$ GABA$_A$Rs. A statistical treatment (unpaired, two-tailed t test) of the single channel currents induced by THIP and GABA revealed that each agonist opened the $\alpha_1\beta_2\gamma_{2S}$ GABA$_A$R to a distinct and significantly different amplitude (P < 0.0001). To explore the observation of differential, agonist-specific single channel current amplitude, we also performed agonist competition experiments on $\alpha_1\beta_2\gamma_{2S}$ GABA$_A$Rs using
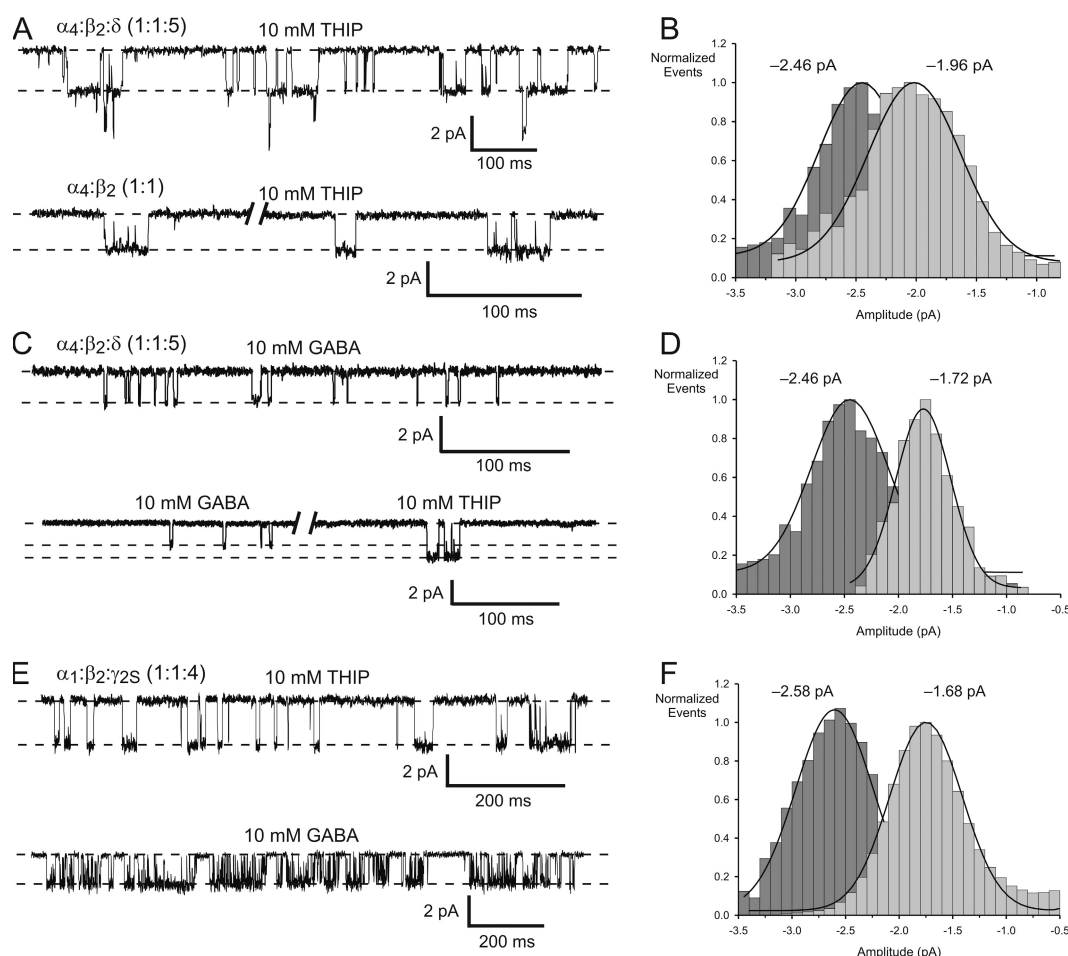
Figure 1. Single channel recordings from GABA$_A$Rs of different subunit compositions in response to GABA and THIP. (A) Two single channel records from patches expressing $\alpha_4\beta_2\delta$ GABA$_A$Rs (above) and $\alpha_4\beta_2$ GABA$_A$Rs (below). The patches were excised from cells transfected with α_4, β_2, and δ subunits at a ratio of 1:1:5 ($\alpha_4{:}\beta_2{:}\delta$) and α_4 and β_2 subunits at a ratio of 1:1 ($\alpha_4{:}\beta_2$), respectively. (B) Pooled amplitude histograms obtained from patches expressing $\alpha_4\beta_2\delta$ GABA$_A$Rs (dark gray; peak = -2.46 ± 0.07 pA, $n = 11$ patches) and $\alpha_4\beta_2$ GABA$_A$Rs (light gray; peak = -1.96 ± 0.06 pA, $n = 16$ patches). (C) A single channel recording from a patch (above) expressing $\alpha_4\beta_2\delta$ GABA$_A$Rs (transfected at 1:1:5) in response to 10 mM GABA and another recording (below) where 10 mM GABA and 10 mM THIP were applied sequentially to the same patch. (D) Pooled amplitude histograms for GABA-gated currents (light gray; peak = -1.72, $n = 3$ patches) and THIP-gated currents (dark gray, transferred from Fig. 1 D from $\alpha_4\beta_2\delta$ GABA$_A$Rs). (E) Single channel activity elicited by THIP (above) and GABA (below) from two separate patches expressing $\alpha_1\beta_2\gamma_{2S}$ GABA$_A$Rs, transfected at a ratio of 1:1:4. (F) Pooled amplitude histograms from patches expressing $\alpha_1\beta_2\gamma_{2S}$ GABA$_A$Rs in response to GABA (light gray; peak = -1.68 pA, $n = 9$ patches) and THIP (dark gray; peak = -2.58 ± 0.08 pA, $n = 10$ patches). Currents were filtered to 2 kHz for display purposes. The peaks corresponding to zero current were omitted for clarity.

GABA and THIP. The agonist application protocol involved coapplying the two agonists, in addition to applying each agonist separately, to the same patch. The experiments were done with the following pairs of agonist concentrations: 5 mM GABA and 5 mM THIP, 5 mM GABA and 100 μM THIP, and, finally, 50 μM GABA and 5 mM THIP (all at -70 mV). As shown in Fig. S1 (available at http://www.jgp.org/cgi/content/full/jgp.200709871/DC1), when 5 mM GABA and 5 mM THIP were coapplied the resulting current amplitude (-2.24 ± 0.05 pA) was not distinguishable from that of THIP alone (-2.22 ± 0.06 pA, P = 0.8431, paired t test). In contrast, the amplitude elicited by 5 mM GABA alone was -1.62 ± 0.02 pA ($n = 4$ patches, Fig. S1 A and Table S1), which an

ANOVA test (one-way with repeated measures) revealed as significantly smaller (P < 0.0001). An example of the second type of competition experiment is shown in Fig. S1 B. Here, when 5 mM THIP was applied alone or in combination with 50 μM GABA, the current amplitudes were indistinguishable, being -2.44 ± 0.04 pA for THIP and -2.47 ± 0.03 pA for THIP plus GABA (P = 0.5559, paired t test). 50 μM GABA applied alone produced an amplitude of -1.70 ± 0.03 ($n = 8$ patches), which again was significantly smaller than when the patches were exposed to 5 mM THIP alone or in combination with GABA (ANOVA, P < 0.0001, Table S1). Fig. S1 C shows recordings from a patch where 5 mM GABA and 100 μM THIP were either applied separately or coapplied.

TABLE I
Unitary Conductance and Kinetic Parameters for $\alpha_4\beta_2\delta$ and $\alpha_1\beta_2\gamma_{2S}$ GABA$_A$Rs

		$\alpha_4\beta_2\delta$	$\alpha_1\beta_2\gamma_{2S}$
Unitary conductance (pS)	THIP	35.5	37.2
	GABA	24.6	25.0
β (s^{-1})	THIP	1624 ± 223	458 ± 18
	GABA	442 ± 100	1799 ± 30
Low concentration burst duration (ms)	THIP	2.30 ± 0.07	4.95 ± 1.30
	GABA	ND	5.38 ± 1.21
k_{obs} EC$_{50}$ (μM)	THIP	1640 ± 160	696 ± 48
	GABA	ND	704 ± 50

ND, not determined

In contrast to saturating concentrations of THIP, 100 μM THIP elicited an amplitude of -1.80 ± 0.03 pA, which was not statistically different from that elicited by 5 mM GABA alone (-1.73 ± 0.05 pA) or 5 mM GABA with 100 μM THIP (-1.78 ± 0.04, $n = 8$ patches, AVOVA, P = 0.2429, Table S1). It is also noteworthy that the current amplitude evoked by 5 mM and 50 μM GABA and 100 μM THIP were not significantly different from each other (ANOVA, P = 0.2125). In three patches we were also able to obtain enough spontaneous (agonist-free) single channel openings to construct reliable amplitude histograms (unpublished data). These measurements yielded an amplitude of -1.60 ± 0.06 pA, which was not significantly different from GABA-gated openings (paired t test, P = 0.3781). Fig. S1 D shows single channel activity from a patch that exhibited some spontaneous openings and was subsequently and sequentially exposed to GABA (50 μM), THIP (100 μM), and THIP (5 mM).

To further characterize single channel current amplitude elicited by the two agonists, we recorded activity at pipette potentials of -70 and $+70$ mV, from the same patch, using either saturating concentrations of GABA or THIP (5 mM) or subsaturating concentrations of GABA (50 μM) or THIP (100 μM). Examples of these experiments are provided in Fig. S2. For reference, the amplitude measurements and statistical comparisons are tabulated in Table S2, along with a measure of current rectification (rectification index, RI), defined as the ratio of single channel current amplitude measured at pipette potentials of -70 and $+70$ mV.

Saturating concentrations of THIP (5 mM) applied to $\alpha_1\beta_2\gamma_{2S}$ GABA$_A$Rs produced similar single channel current amplitude at -70 mV (-2.32 ± 0.07 pA) and $+70$ mV (2.30 ± 0.07 pA, paired t test, P = 0.839, $n = 8$ patches, Fig. S2 A), resulting in an RI of $\sim$1. 100 μM THIP elicited a significantly greater current amplitude at -70 mV (-1.76 ± 0.11 pA) than at $+70$ mV (1.46 ± 0.03 pA, paired t test, P = 0.038, $n = 5$ patches, Fig. S2 B), producing slight inward rectification (RI = 1.10). This was also the case when using GABA as the agonist at both saturating and subsaturating concentrations. 5 mM GABA elicited a current amplitude of -1.66 ± 0.06 pA at -70

mV and 1.45 ± 0.04 pA at $+70$ mV ($n = 8$ patches, paired t test, P = 0.025, RI = 1.14, Fig. S2 C). Similarly, 50 μM GABA elicited a current amplitude of -1.74 ± 0.06 pA at -70 mV and 1.40 ± 0.10 pA at $+70$ mV ($n = 3$ patches, paired t test, P = 0.003, RI = 1.24; Fig. S2 D, Table S2).

Using Eq. 3, single channel currents of -2.46 and -1.70 pA activated by THIP and GABA, respectively, and corresponding reversal potentials (unpublished data) for the two agonists, we calculated the unitary conductance of $\alpha_4\beta_2\delta$ GABA$_A$Rs. The calculations yielded conductances of 35.5 and 24.6 pS for THIP and GABA, respectively, at -70 mV. Similar calculations for $\alpha_1\beta_1\gamma_{2S}$ GABA$_A$Rs produced conductance values of 37.2 pS for THIP and 25.0 pS for GABA (Table I).

For subsequent single channel analysis of $\alpha_4\beta_2\delta$ GABA$_A$Rs we focused on the THIP-activated -2.46 pA current, and for $\alpha_1\beta_2\gamma_{2S}$ GABA$_A$Rs, the THIP-activated -2.58 pA and GABA-activated -1.68 pA activity. Due to its rarity, and the possibility that the lower conductance, GABA-gated activity in $\alpha_1\beta_2\gamma_{2S}$ GABA$_A$Rs could be mediated by binary $\alpha_1\beta_2$ channels (Wagner et al., 2004; Li et al., 2006), which were ~-1.1 pA, we decided not to analyze these particular currents any further.

Current Activation Rates in $\alpha_4\beta_2\delta$ and $\alpha_1\beta_2\gamma_{2S}$ GABA$_A$Rs are Agonist Dependent

Current activation was examined over a range of concentrations of GABA and THIP for $\alpha_4\beta_2\delta$ and $\alpha_1\beta_2\gamma_{2S}$ GABA$_A$Rs, using ultrafast agonist application on excised outside-out patches. For $\alpha_4\beta_2\delta$ GABA$_A$Rs in response to GABA, data from small cells were also included, as these generally gave larger currents with improved signal–noise ratios. However, in spite of our efforts, it was only possible to obtain reliable activation rate data for the higher concentrations or GABA (10, 20, and 30 mM) for these channels.

The rate of current activation was measured by fitting Eq. 1 to the onset phase of the current (Fig. 2, A and B), from which the observed activation rate constant (k_{obs}) was obtained. k_{obs} was then plotted as a function of agonist concentration over the entire range of concentrations tested (Fig. 2, C and D). The resulting data were fitted to
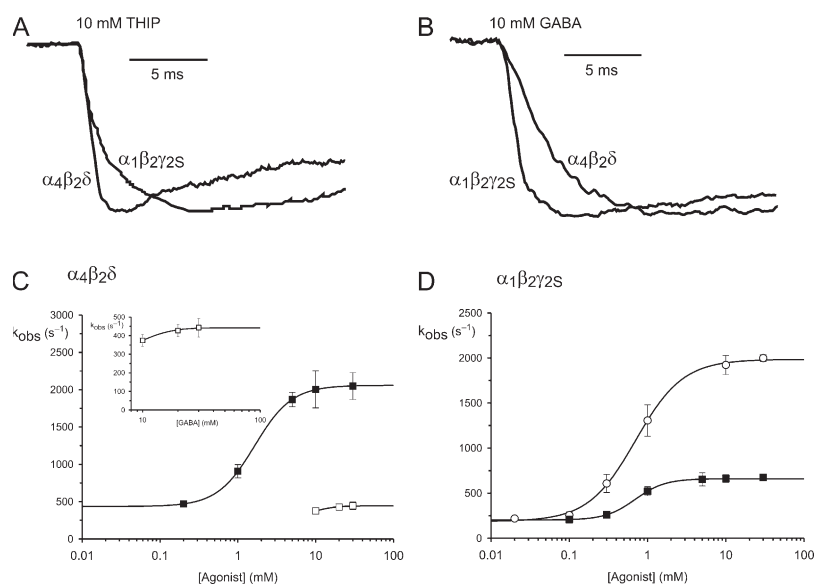
Figure 2. Current activation rates for $\alpha_4\beta_2\delta$ and $\alpha_1\beta_2\gamma_{2S}$ GABA$_A$Rs in response to THIP and GABA. (A) The activation phase of currents mediated by $\alpha_4\beta_2\delta$ and $\alpha_1\beta_2\gamma_{2S}$ GABA$_A$Rs in response to fast agonist application of THIP, showing that THIP activates $\alpha_4\beta_2\delta$ GABA$_A$Rs more rapidly. (B) The activation phase of currents for $\alpha_4\beta_2\delta$ and $\alpha_1\beta_2\gamma_{2S}$ GABA$_A$Rs in response to fast application of GABA, showing that $\alpha_1\beta_2\gamma_{2S}$ GABA$_A$Rs activate more rapidly. (C) Plot of activation rate constant (k_{obs}) versus [agonist] for $\alpha_4\beta_2\delta$ GABA$_A$Rs. The plot for GABA-gated activation is shown on an expanded scale (inset). (D) Plot of activation rate constant (k_{obs}) versus [agonist] for $\alpha_1\beta_2\gamma_{2S}$ GABA$_A$Rs. The data points were fitted to a modified form of the Hill equation (see Materials and methods). The parameters of the fit are shown in Table I. THIP, black symbols; GABA, white symbols.

a Hill type equation (Eq. 2) to obtain the upper and lower asymptotic levels and the concentration that elicits the half-maximal k_{obs} (k_{obs} EC$_{50}$; Table I). For both agonists the k_{obs} increased with increasing agonist concentration, plateauing to a maximum at ~10–20 mM for both agonists. For $\alpha_4\beta_2\delta$ GABA$_A$Rs, the k_{obs} was greater for THIP than GABA, reaching a maximum for the two agonists of 2058 s^{-1} and 442 s^{-1}, respectively (Fig. 2 C). The converse was the case for $\alpha_1\beta_2\gamma_{2S}$ GABA$_A$Rs, with GABA producing a higher activation rate constant than THIP. The maximum k_{obs} value for GABA was 1986 s^{-1} and for THIP was 660 s^{-1} (Fig. 2 D). The maximum activation rate constant for GABA-gated $\alpha_1\beta_2\gamma_{2S}$ GABA$_A$Rs, estimated from medium-sized cells (Keramidas et al., 2006), is comparable, although slightly lower than that obtained here from excised patches using the same ultrafast perfusion system.

With decreasing agonist concentration, current activation became increasingly slower, plateauing to distinct, nonzero asymptotic levels. For $\alpha_4\beta_2\delta$ channels activated by THIP, the lower asymptote was 434 s^{-1}. For $\alpha_1\beta_2\gamma_{2S}$ channels the lower asymptote k_{obs} values were 202 s^{-1} and 186 s^{-1} for THIP and GABA, respectively. These values were not significantly different (Table I).

The agonist concentration that produced the half maximal k_{obs} values (k_{obs} EC$_{50}$) varied with channel type. $\alpha_4\beta_2\delta$ channels had a k_{obs} EC$_{50}$ for THIP of 1.64 mM. $\alpha_1\beta_2\gamma_{2S}$ GABA$_A$Rs had statistically indistinguishable k_{obs} EC$_{50}$s, which were 696 μM for THIP and 704 μM for GABA (Table I). These results indicate that $\alpha_4\beta_2\delta$ GABA$_A$Rs have a lower apparent affinity for THIP than $\alpha_1\beta_2\gamma_{2S}$ GABA$_A$Rs.

Simulating Macroscopic Currents and Simple Kinetic Schemes

To obtain estimates of rate constants in Scheme 1 for both channels and agonist we fitted simulated currents

to real macropatch currents in response to 1–2-ms applications of 30 mM agonist, as previously described (Keramidas et al., 2006). To improve the accuracy of the fit and reduce the number of free parameters in the fitting procedure, we imposed the following constraints on our simulations. These constraints were based on experimentally derived parameters obtained from the k_{obs} versus concentration plots (Table I). First, we set the opening rate constant (β) in Scheme 1 to equal the estimated value for β^* from the k_{obs} plot, after subtracting the lower asymptotic value (Maconochie et al., 1994; Keramidas et al., 2006) and fixed this parameter in the fitting procedure. Second, we took our experimental k_{obs} EC$_{50}$ values to be reasonable estimates of the equilibrium dissociation constant for the second binding step in Scheme 1 ($K_d = 2k_{-1}/k_{+1}$), after making a minor correction for equivalent and independent binding sites (Maconochie and Steinbach, 1998), which we assumed. This gave us a ratio of dissociation rate constant to association rate constant (k_{-1}/k_{+1}), which we fixed during the simulations, allowing effectively only the k_{+1} value itself to vary in the simulations of $\alpha_1\beta_2\gamma_{2S}$ GABA$_A$R currents and THIP-activated $\alpha_4\beta_2\delta$ GABA$_A$R currents. When simulating GABA-activated $\alpha_4\beta_2\delta$ GABA$_A$R currents we set β to the upper asymptote (although this is likely an overestimate) and allowed k_{-1} and k_{+1} to vary freely as our GABA-gated k_{obs} plot did not extend far enough to obtain a lower asymptote or k_{obs} EC$_{50}$, respectively. In addition, we estimated the channel open probability ($P_O^{macropatch}$) in response to 1–2-ms exposure to agonist using nonstationary fluctuation analysis. The $P_O^{macropatch}$ values we obtained were, for $\alpha_4\beta_2\delta$ GABA$_A$Rs, GABA–0.25 and THIP–0.36, and for $\alpha_1\beta_2\gamma_{2S}$ GABA$_A$Rs, GABA–0.56 and THIP–0.42 (unpublished data). The currents were then scaled to the $P_O^{macropatch}$ values before generating the
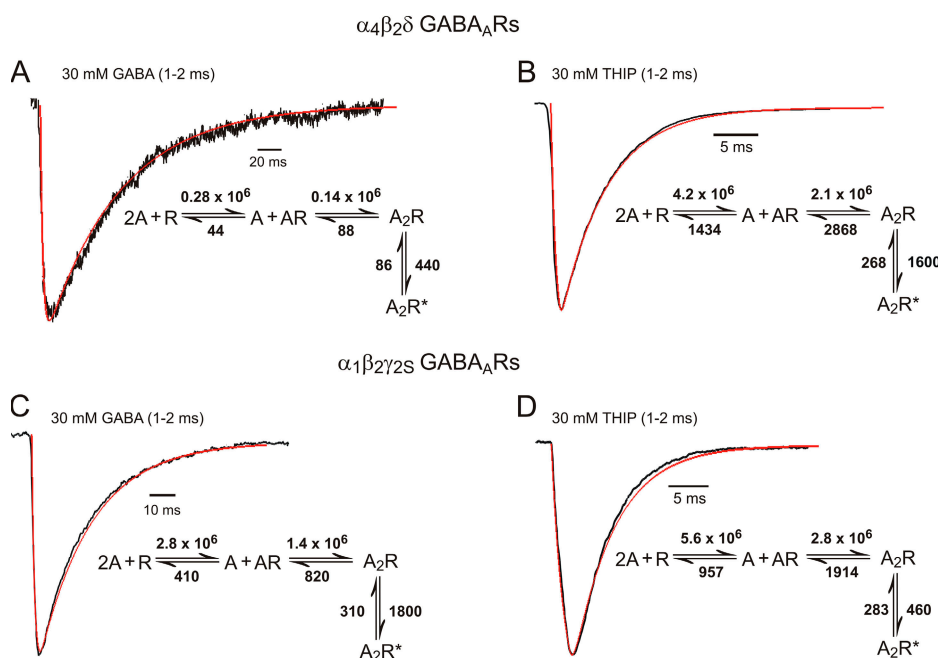
$\alpha_4\beta_2\delta$ GABA$_A$Rs

A 30 mM GABA (1-2 ms)

20 ms

$$2A + R \underset{44}{\overset{0.28 \times 10^6}{\rightleftharpoons}} A + AR \underset{88}{\overset{0.14 \times 10^6}{\rightleftharpoons}} A_2R$$

$$A_2R \underset{86}{\overset{440}{\rightleftharpoons}} A_2R^*$$

B 30 mM THIP (1-2 ms)

5 ms

$$2A + R \underset{1434}{\overset{4.2 \times 10^6}{\rightleftharpoons}} A + AR \underset{2868}{\overset{2.1 \times 10^6}{\rightleftharpoons}} A_2R$$

$$A_2R \underset{268}{\overset{1600}{\rightleftharpoons}} A_2R^*$$

$\alpha_1\beta_2\gamma_{2S}$ GABA$_A$Rs

C 30 mM GABA (1-2 ms)

10 ms

$$2A + R \underset{410}{\overset{2.8 \times 10^6}{\rightleftharpoons}} A + AR \underset{820}{\overset{1.4 \times 10^6}{\rightleftharpoons}} A_2R$$

$$A_2R \underset{310}{\overset{1800}{\rightleftharpoons}} A_2R^*$$

D 30 mM THIP (1-2 ms)

5 ms

$$2A + R \underset{957}{\overset{5.6 \times 10^6}{\rightleftharpoons}} A + AR \underset{1914}{\overset{2.8 \times 10^6}{\rightleftharpoons}} A_2R$$

$$A_2R \underset{283}{\overset{460}{\rightleftharpoons}} A_2R^*$$

Figure 3. Current simulations of macroscopic currents in response to fast application of agonist. Examples of macropatch currents recorded from patches expressing $\alpha_4\beta_2\delta$ GABA$_A$Rs in response to a 1-ms exposure of 30 mM GABA (A) and 30 mM THIP (B) with superimposed simulated currents. Accompanying the current–simulation pairs are simple kinetic schemes with the average rate constants obtained from three to four patches each. Examples of macropatch currents recorded from patches expressing $\alpha_1\beta_2\gamma_{2S}$ GABA$_A$Rs in response to a 1-ms exposure of 30 mM GABA (C) and 30 mM THIP (D) with superimposed simulated currents.

simulations. Fig. 3 shows examples of real currents and the superimposed simulated currents generated with the above fitting constraints. Accompanying each real and simulated current pair is the corresponding kinetic scheme and averaged rate constants (from three to four patches each) for both GABA$_A$Rs and agonists. The rate constants estimated in Scheme 1 for GABA-activated $\alpha_4\beta_2\delta$ GABA$_A$Rs were (Fig. 3 A; β was set to 440 s^{-1}) $\alpha = 86 \pm 6$ s^{-1}, $k_{+1} = 0.14 \pm 0.06 \times 10^6$ M^{-1}s^{-1}, and $k_{-1} = 44 \pm 3$ s^{-1}, and for THIP-activated $\alpha_4\beta_2\delta$ GABA$_A$Rs (Fig. 3 B; β was set to 1600 s^{-1}), $\alpha = 268 \pm 17$ s^{-1}, $k_{+1} = 2.1 \pm 0.3$ M^{-1}s^{-1}, and $k_{-1} = 1434 \pm 26$ s^{-1}. For THIP-activated $\alpha_1\beta_2\gamma_{2S}$ GABA$_A$Rs, the rate constants were (Fig. 3 C; β was set to 460 s^{-1}) $\alpha = 283 \pm 5$ s^{-1}, $k_{+1} = 3.3 \pm 0.2$ 10^6 M^{-1}s^{-1}, and $k_{-1} = 957 \pm 12$ s^{-1}, and for GABA-activated $\alpha_1\beta_2\gamma_{2S}$ GABA$_A$Rs (Fig. 3 D; β was set to 1800 s^{-1}), $\alpha = 310 \pm 14$ s^{-1}, $k_{+1} = 1.4 \pm 0.2 \times 10^6$ M^{-1}s^{-1}, and $k_{-1} = 410 \pm 22$ s^{-1}.

Single Channel Burst Characteristics Are Determined by Agonist Type

To obtain information about gating kinetics of fully liganded channels, we used saturating concentrations of THIP and GABA (10 mM) to elicit single channel currents in $\alpha_4\beta_2\delta$ and $\alpha_1\beta_2\gamma_{2S}$ GABA$_A$Rs. THIP activated $\alpha_4\beta_2\delta$ GABA$_A$Rs more consistently and produced more complex bursts than GABA (Fig. 4 A and Fig. 6 A), so we focused most of our efforts on the THIP-activated activity. Segments (clusters) of THIP-activated activity were divided into bursts by applying a critical shut time (t_{crit}), which ranged between 17 and 37 ms. Table II summarizes the mean burst durations and intraburst open probability (P_O) for $\alpha_4\beta_2\delta$ GABA$_A$Rs activated by THIP and GABA. As can be seen from Table II and Fig. 4 A and Fig. 6 A, THIP induced bursts of activity in $\alpha_4\beta_2\delta$

GABA$_A$Rs that were of relatively short duration (32.6 ± 4.4 ms) and had an intraburst P_O of 0.40 ± 0.02. GABA-activated bursts were much briefer (7.17 ± 0.58 ms) and had an intraburst P_O of 0.25 ± 0.05. Similar analysis was applied to THIP- and GABA-activated single channel activity in $\alpha_1\beta_2\gamma_{2S}$ GABA$_A$Rs. In response to 10 mM THIP, single channel openings in $\alpha_1\beta_2\gamma_{2S}$ GABA$_A$Rs occurred as short bursts, defined by t_{crit} values that ranged between 17 and 25 ms. These bursts were similar in duration and structure to the THIP-activated activity in $\alpha_4\beta_2\delta$ GABA$_A$Rs (Fig. 4, B and D, and Fig. 7 A). The mean burst duration and intraburst P_O for this activity was 31.6 ± 3.9 ms and 0.47 ± 0.03, respectively (Table II). Notably, THIP induced shorter inactive periods, normally associated with channel desensitization, than GABA at $\alpha_1\beta_2\gamma_{2S}$ GABA$_A$Rs. The range of the longest mean shut duration, measured from three patches in the presence of THIP was ~ 0.5–10 s (Fig. 7), whereas, in the presence of GABA the channels shut for periods ranging from ~ 2 to 200 s ($n = 4$ patches, Fig. 4 C and Fig. 8). These observations suggest that THIP elicits similar bursting patterns at both channels, whereas GABA elicits single channel activity that is substantially different from that elicited by THIP at the same channel.

In addition to longer-lived desensitization, GABA induced long clusters of activity that could be divided into distinct bursting patterns on the basis intraburst P_O. This kinetic phenomenon has recently been reported for $\alpha_1\beta_1\gamma_{2S}$ channels recorded in the intact-patch configuration (Lema and Auerbach, 2006). To our knowledge, the present study is the first to report distinct bursting patterns, or modes, in excised outside-out patches for GABA$_A$Rs. Moreover, our data suggest that bursting modes are agonist specific, with THIP eliciting
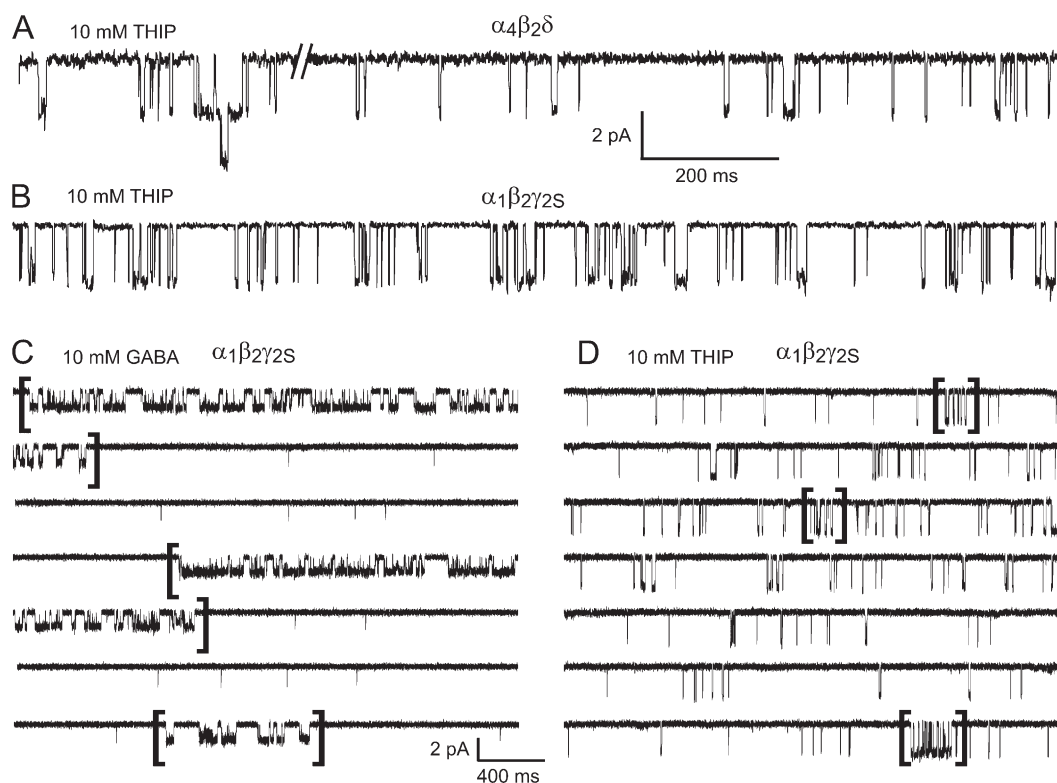
Figure 4. Single channel activity is agonist dependent in $\alpha_4\beta_2\delta$ and $\alpha_1\beta_2\gamma_{2S}$ GABA$_A$Rs. Single channel recordings from patches expressing $\alpha_4\beta_2\delta$ GABA$_A$Rs (A) and $\alpha_1\beta_2\gamma_{2S}$ GABA$_A$Rs (B) in response to THIP. Bursts form both channel types were of relatively short duration (average burst duration <50 ms) and showed no apparent modal bursting. The intraburst open probability (P$_O$) was also similar for both channels, being ∼0.4–0.5. $\alpha_1\beta_2\gamma_{2S}$ GABA$_A$Rs typically opened more frequently than $\alpha_4\beta_2\delta$ GABA$_A$Rs. Continuous 3-s sweeps of single channel recordings from the same patch expressing $\alpha_1\beta_2\gamma_{2S}$ GABA$_A$Rs in response to GABA (C) and THIP (D). Note the absence of long quiescent periods, the larger current amplitude, and shorter clusters of activity (in square parentheses) in the presence of THIP. Currents were filtered to 2 kHz for display purposes.

only one discernable type of bursting mode and GABA eliciting at least two distinct modes. Clusters of GABA-gated activity were separated into modes using "Select" within QuB, as previously described (Lema and Auerbach, 2006). These were extracted to separate files for division into bursts by applying a t$_{crit}$. t$_{crit}$ values were generally shorter for the high P$_O$ bursts. They ranged between 8 and 12 ms and 9 and 17 ms for high (H-Mode) and medium (M-Mode) P$_O$ bursts, respectively. Instances where modal switching occurred within the same cluster were not included in the analysis. Fig. 5 A shows

a channel (presumably the same channel) that enters an M-Mode cluster then switches to an H-Mode cluster. Most patches exhibited two gating modes, with the M-Mode P$_O$ being the most prevalent. The lowest P$_O$ mode (L-Mode) was the least prevalent, occurring only in 3 of 15 patches and was not analyzed any further (Fig. 5 A). The mean burst durations and corresponding intraburst P$_O$s for the H-Mode and M-Mode were as follows: H-Mode, 122.6 ± 19.7 ms and 0.87 ± 0.02 (n = 5 patches); M-Mode, 101.0 ± 8.3 ms and 0.69 ± 0.02 (n = 11 patches, Table II).

TABLE II

Single Channel Burst Properties for $\alpha_4\beta_2\delta$ and $\alpha_1\beta_2\gamma_{2S}$ GABA$_A$Rs

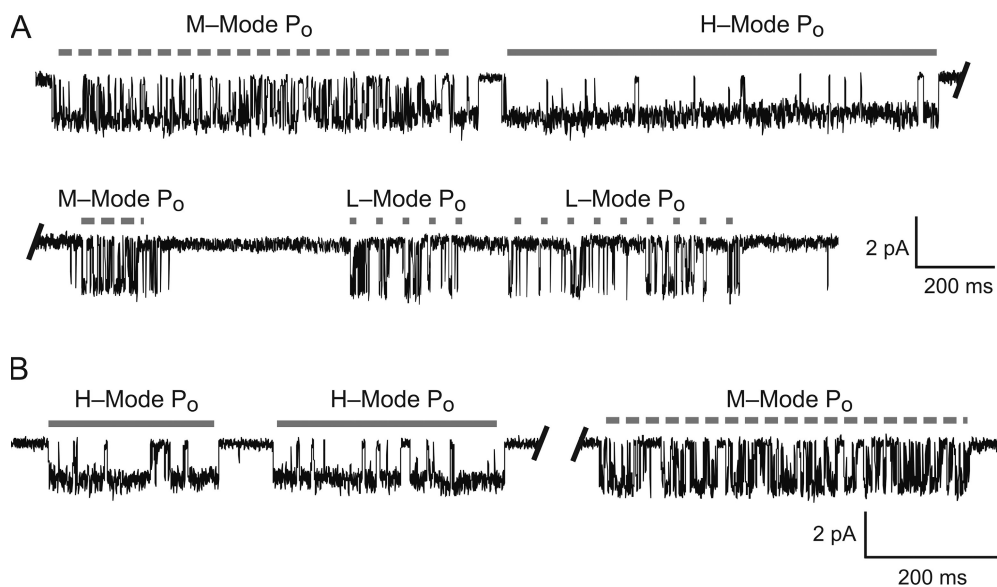|	$\alpha_4\beta_2\delta$ (n)	$\alpha_1\beta_2\gamma_{2S}$ (n)	
	THIP	THIP	
Burst duration (ms)	32.6 ± 4.4 (9)	31.6 ± 3.9 (7)	
Intraburst P$_O$	0.40 ± 0.02 (9)	0.47 ± 0.03 (7)	
	GABA	GABA	
Burst duration (ms)	7.17 ± 0.58 (3)	H-Mode	M-Mode
		122.6 ± 19.7 (5)	101.0 ± 8.3 (11)
Intraburst P$_O$	0.25 ± 0.05 (3)	0.87 ± 0.02 (5)	0.69 ± 0.02 (11)

Figure 5. GABA elicits bursting modes in $\alpha_1\beta_2\gamma_{2S}$ GABA$_A$Rs. (A) A patch exhibiting medium mode (M-Mode P$_O$), high mode (H-Mode P$_O$), and low mode (L-Mode P$_O$) clusters in the presence of 10 mM GABA. (B) Another patch exhibiting only the H-Mode P$_O$ and M-Mode P$_O$ gating patterns. Currents were filtered to 2 kHz for display purposes.

Single Channel Burst Analysis

We used saturating agonist concentrations (10 mM) to model gating kinetics in $\alpha_4\beta_2\delta$ GABA$_A$Rs in response to THIP and $\alpha_1\beta_2\gamma_{2S}$ GABA$_A$Rs in response to THIP and GABA. Fig. 6 shows an example of THIP-activated activity in $\alpha_4\beta_2\delta$ GABA$_A$Rs and the accompanying dwell histograms for bursts. As can be seen in the figure, the data were best fit with two shut and two open components. The corresponding mean time constants (and fractions) for each exponential component, from five patches, are shown in Table III.

THIP-activated bursts in $\alpha_1\beta_2\gamma_{2S}$ GABA$_A$Rs were also described best with a mixture of two open and two shut components (Fig. 7, $n = 3$ patches), strongly suggesting that THIP elicits similar activation kinetics in both channels. The main difference in the time constants between the two channels was that the first shut time constant (τ_{C1}) was nearly threefold greater and over twofold more prevalent for $\alpha_1\beta_2\gamma_{2S}$ GABA$_A$Rs. GABA-gated bursts required three shut and three open components to adequately describe M-Mode activation (Fig. 8, $n = 10$ patches). This is the same number of components reported for $\alpha_1\beta_1\gamma_{2S}$ GABA$_A$Rs (Lema and Auerbach, 2006). For the H-Mode activity, only two shut and three open components were required (Fig. 9, $n = 5$ patches), in contrast to that reported by Lema and Auerbach (2006). Notably, the longest open time constant in H-Mode activity was over 2.5–fold longer than the corresponding time constant in the M-Mode activity.

More Complex Gating Schemes

Postulated schemes for both channels and agonists included single gateway and multi-gateway routes to open states. Generally, multi-gateway schemes, such as Shut–Open–Shut–Open, produced either lower LL scores than single gateway schemes or computed rate constants

that were incompatible with the simpler schemes derived from macropatch currents. As an additional means of determining the best schemes we simulated macropatch data using the three complex schemes that had the highest LL values for each experimental condition.

THIP-gated activity in both channels could be described by similar schemes. The similarities included the number of open and shut states and a common pathway between the first shut and the first open state, $A_2R^1 \leftrightarrow A_2R^{1*}$ (Fig. 10, A and B). The opening rate constants between these two states were consistent with but somewhat higher than those obtained from our macropatch experiments (refer to Fig. 3). For $\alpha_4\beta_2\delta$ channels, the next best scheme produced similar opening rate constants ($\beta \sim 2000$ s^{-1}), had LL values that were similar to and not significantly different from the best scheme (*t* test, P > 0.05, $n = 5$), but did not reproduce macropatch currents (especially the deactivation phase) as adequately as the best scheme. For $\alpha_1\beta_2\gamma_{2S}$ GABA$_A$Rs, the best rival scheme had LL values that were only $\sim$10 units lower, but not significantly so (P < 0.05, $n = 10$), produced opening rate constants that were too high, and was not able to closely simulate macropatch currents.

GABA-gated activation in $\alpha_1\beta_2\gamma_{2S}$ GABA$_A$Rs included three shut and three open states for the M-Mode activity (Fig. 10 C) and two shut and three open states for the H-Mode activity (Fig. 10 D). There were two notable features that were common in both schemes derived for the two gating modes. First, in both schemes the channels entered a second shut state before the first open state ($A_2R^1 \leftrightarrow A_2R^2 \leftrightarrow A_2R^{1*}$). Second, the opening rate leading to the first open state was comparable between the two modes (Fig. 11, C and D), although somewhat lower for H-Mode activity. Rival schemes for both gating modes for these channels were difficult to rank. The schemes that rivaled those presented in Fig. 10 had LL
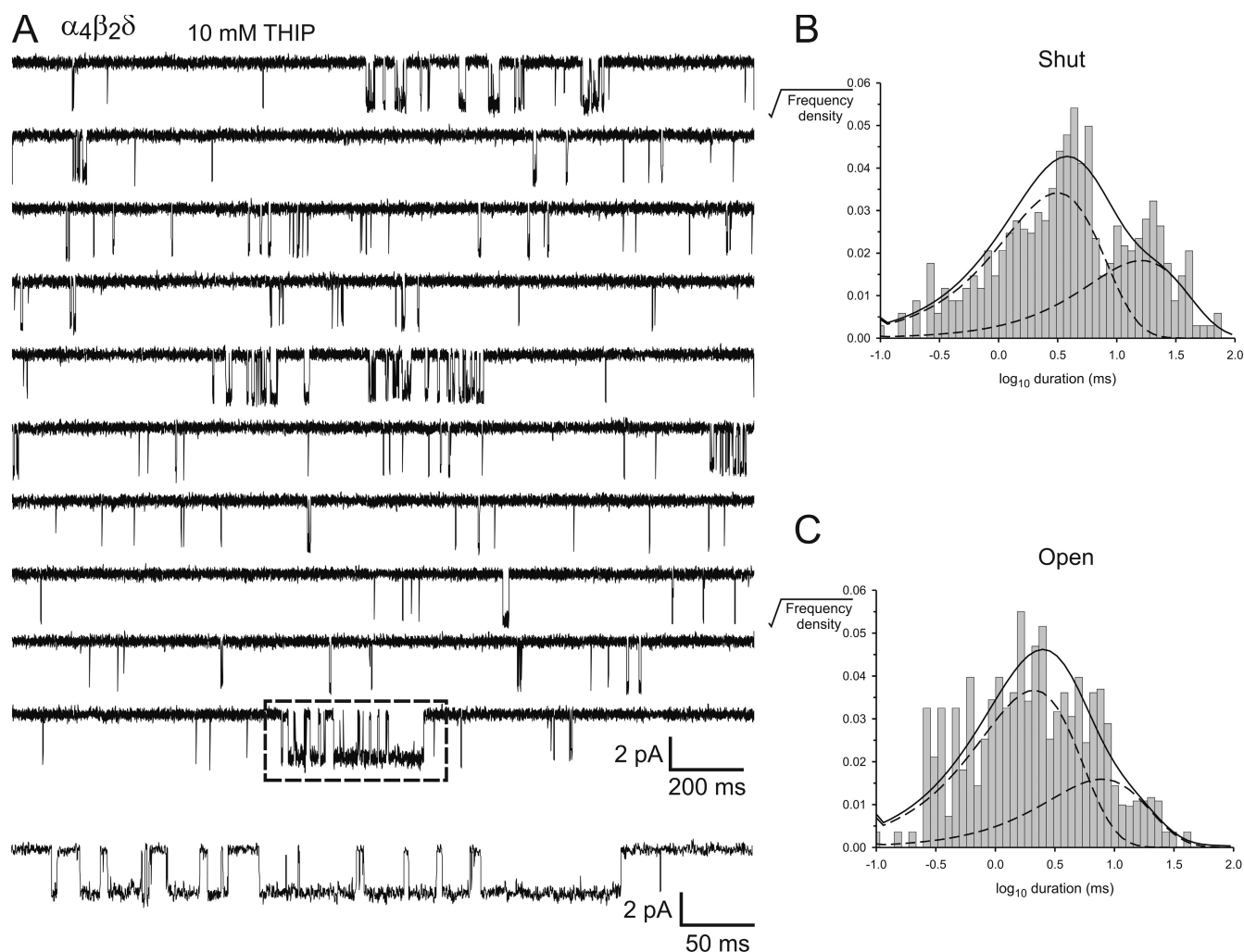
Figure 6. Burst analysis of THIP-activated $\alpha_4\beta_2\delta$ GABA$_A$Rs. (A) Continuous, 2-s sweeps of single channel activity recorded from a patch expressing $\alpha_4\beta_2\delta$ GABA$_A$Rs in response to 10 mM THIP. Enclosed in the box is a long cluster, which is shown on an expanded scale below. (B) Dwell time histogram of apparent shut intervals and (C) dwell time histogram of apparent open intervals for the activity shown in A. Distributions were fit with a mixture of exponential probability density functions (dark lines). The individual components are shown as broken lines. The analysis revealed two shut and two open components for this activity. Currents were filtered to 2 kHz for display purposes.

values that differed by <20 units and were not significantly different (P > 0.05, $n = 5$). The main difference was that the schemes presented in Fig. 10 produced β values that were similar to the simple schemes, and could adequately simulate macropatch currents.

DISCUSSION

The primary objectives of this study were to investigate and compare the kinetics of channel activation of $\alpha_4\beta_2\delta$ and $\alpha_1\beta_2\gamma_{2S}$ GABA$_A$Rs within the context of kinetic schemes. Throughout the investigation, THIP (Gaboxadol) was used in addition to GABA because THIP elicited single channel currents in GABA$_A$Rs containing extrasynaptic subunits (e.g., the α_4 subunit) more reliably than GABA. This enabled a comparison of the effects on channel kinetics, and unexpectedly, conductance, of both channels in response to the two agonists.

Single Channel Heterogeneity in GABA$_A$Rs

Our initial attempts at recording and identifying $\alpha_4\beta\delta$ GABA$_A$R currents on a single channel level revealed that a transfection ratio of 1:1:2 (α_4:β_2:δ) resulted in current heterogeneity. This observation was both intriguing and potentially confounded the feasibility of the study. Transfections at different subunit ratios and combinations were used to elucidate the basis for this heterogeneity and aid in identifying the ternary $\alpha_4\beta_2\delta$ GABA$_A$R. This phase of the study yielded recordings of single channel, THIP-activated currents mediated by binary GABA$_A$Rs composed of α_4 and β_2 subunits. To our knowledge these are the first recordings of these GABA$_A$Rs on a single channel level. Increasing the amount of δ subunit in our transfections to 1:1:5 resulted in a marked reduction in single channel current heterogeneity. Recordings in response to THIP from these transfections revealed a preponderance of single channel openings

TABLE III

Burst Analysis for $\alpha_4\beta_2\delta$ and $\alpha_1\beta_2\gamma_{2S}$ GABA$_A$Rs

		τ_{C1} (ms) [A_{C1}]	τ_{C2} (ms) [A_{C2}]	τ_{C3} (ms) [A_{C3}]	τ_{O1} (ms) [A_{O1}]	τ_{O2} (ms) [A_{O2}]	τ_{O3} (ms) [A_{O3}]
$\alpha_4\beta_2\delta$	10 mM THIP ($n = 5$)	1.04 ± 0.47 [0.31 ± 0.10]	14.9 ± 4.8 [0.69 ± 0.10]	–	1.76 ± 0.57 [0.49 ± 0.10]	7.70 ± 2.03 [0.51 ± 0.11]	–
	10 mM THIP ($n = 3$)	2.98 ± 0.31 [0.74 ± 0.06]	18.3 ± 2.3 [0.26 ± 0.06]	–	2.16 ± 0.70 [0.34 ± 0.11]	6.76 ± 1.29 [0.66 ± 0.11]	–
$\alpha_1\beta_2\gamma_{2S}$		M–Mode ($n = 10$)					
	10 mM GABA	0.26 ± 0.02 [0.48 ± 0.03]	1.12 ± 0.14 [0.31 ± 0.03]	3.87 ± 0.41 [0.21 ± 0.03]	0.49 ± 0.02 [0.26 ± 0.03]	2.58 ± 0.09 [0.49 ± 0.04]	5.17 ± 0.38 [0.25 ± 0.04]
		H–Mode ($n = 5$)					
		0.34 ± 0.04 [0.58 ± 0.05]	1.94 ± 0.22 [0.42 ± 0.03]	–	0.59 ± 0.11 [0.18 ± 0.02]	4.22 ± 0.73 [0.41 ± 0.03]	13.2 ± 2.6 [0.41 ± 0.05]

to ∼−2.5 pA, which were statistically different from currents recorded from transfecting only α_4 and β_2 subunits. This observation strongly suggested that a transfection ratio of 1:1:5 favored the inclusion of the δ subunit in the expressed channels, and we inferred that these channels were the desired $\alpha_4\beta_2\delta$ GABA$_A$Rs. Subsequent
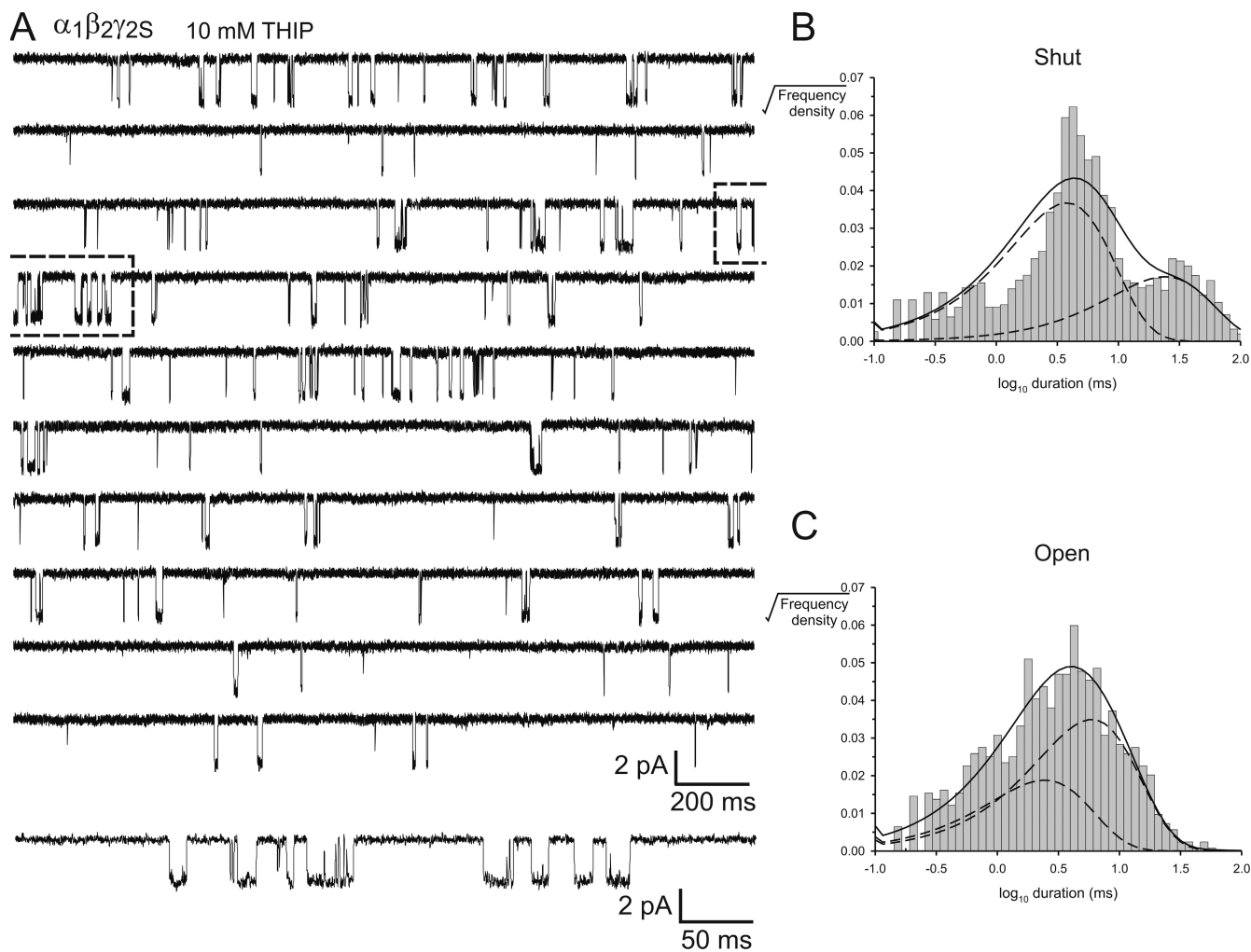

Figure 7. Burst analysis of THIP-activated $\alpha_1\beta_2\gamma_{2S}$ GABA$_A$Rs. (A) Continuous, 2-s sweeps of single channel activity recorded from a patch expressing $\alpha_1\beta_2\gamma_{2S}$ GABA$_A$R in response to 10 mM THIP. The cluster enclosed in the box is expanded below. (B) Dwell time histogram of apparent shut intervals and (C) dwell time histogram of apparent open intervals for the activity shown in A. Distributions were fit with a mixture of exponential probability density functions (dark lines). The individual components are shown as broken lines. The analysis revealed two shut and two open components for this activity. Currents were filtered to 2 kHz for display purposes.
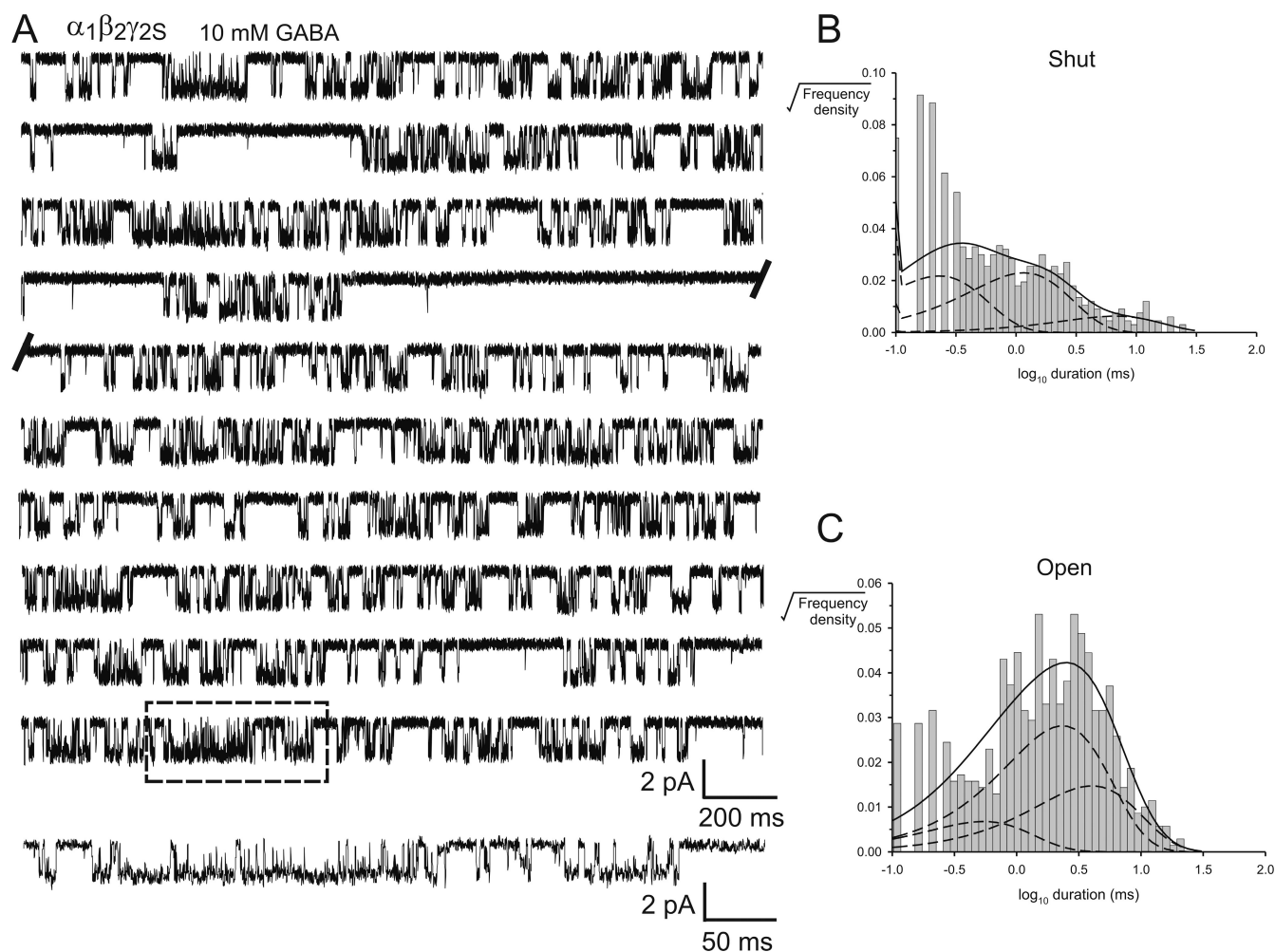
Figure 8. Burst analysis of M-Mode activity in $\alpha_1\beta_2\gamma_{2S}$ GABA$_A$Rs. (A) Continuous, 2-s sweeps of single channel activity recorded from a patch expressing $\alpha_1\beta_2\gamma_{2S}$ GABA$_A$R in response to 10 mM GABA. The break in the recording represents $\sim$2 min of no activity ("desensitization"). The segment enclosed in the box is expanded below. (B) Dwell time histogram of apparent shut intervals and (C) dwell time histogram of apparent open intervals for the activity shown in A. Distributions were fit with a mixture of exponential probability density functions (dark lines). The individual components are shown as broken lines. The analysis revealed three shut and three open components for this activity. Currents were filtered to 2 kHz for display purposes.

experiments, including macropatch recordings, on $\alpha_4\beta_2\delta$ GABA$_A$Rs were performed on cells transfected at a ratio of 1:1:5.

Transfections of α_1, β_2, and γ_{2S} subunits at a ratio of 1:1:4 also resulted in some heterogeneity, but only in response to GABA, which elicited openings of ~ -1.7 pA and ~ -1.1 pA. The latter openings were rare and not subjected to single channel analysis on the grounds that they may have been mediated by binary $\alpha_1\beta_2$ GABA$_A$Rs, as previously reported (Wagner et al., 2004; Li et al., 2006).

Agonist Type and Concentration Determine Single Channel Current Amplitude

In the course of our single channel measurements, we also made the novel discovery that THIP and GABA opened the two channels to different conductance levels. For both $\alpha_4\beta_2\delta$ and $\alpha_1\beta_2\gamma_{2S}$ GABA$_A$Rs (at -70 mV), saturating concentrations of THIP consistently evoked

$\sim$35–37-pS openings in both channels, whereas the same concentration of GABA evoked $\sim$25-pS openings in both channels. The veracity of this observation was especially compelling when THIP and GABA were applied to the same patch, sequentially, including cases where there was no evidence of multiple channels within the patch. On further investigation it became apparent that subsaturating concentrations of THIP evoked single channels openings that were of the same amplitude as GABA-gated currents at saturating and subsaturating concentrations (when tested on $\alpha_1\beta_2\gamma_{2S}$ GABA$_A$Rs). Consistent with previous reports of single channel conductance (Mortensen et al., 2004; Lema and Auerbach, 2006), low and high concentrations of GABA produced the same current amplitude. The experiments in the present study clearly show that only high concentrations of THIP produce high conductance openings. Our straightforward interpretation of this finding is that different degrees of
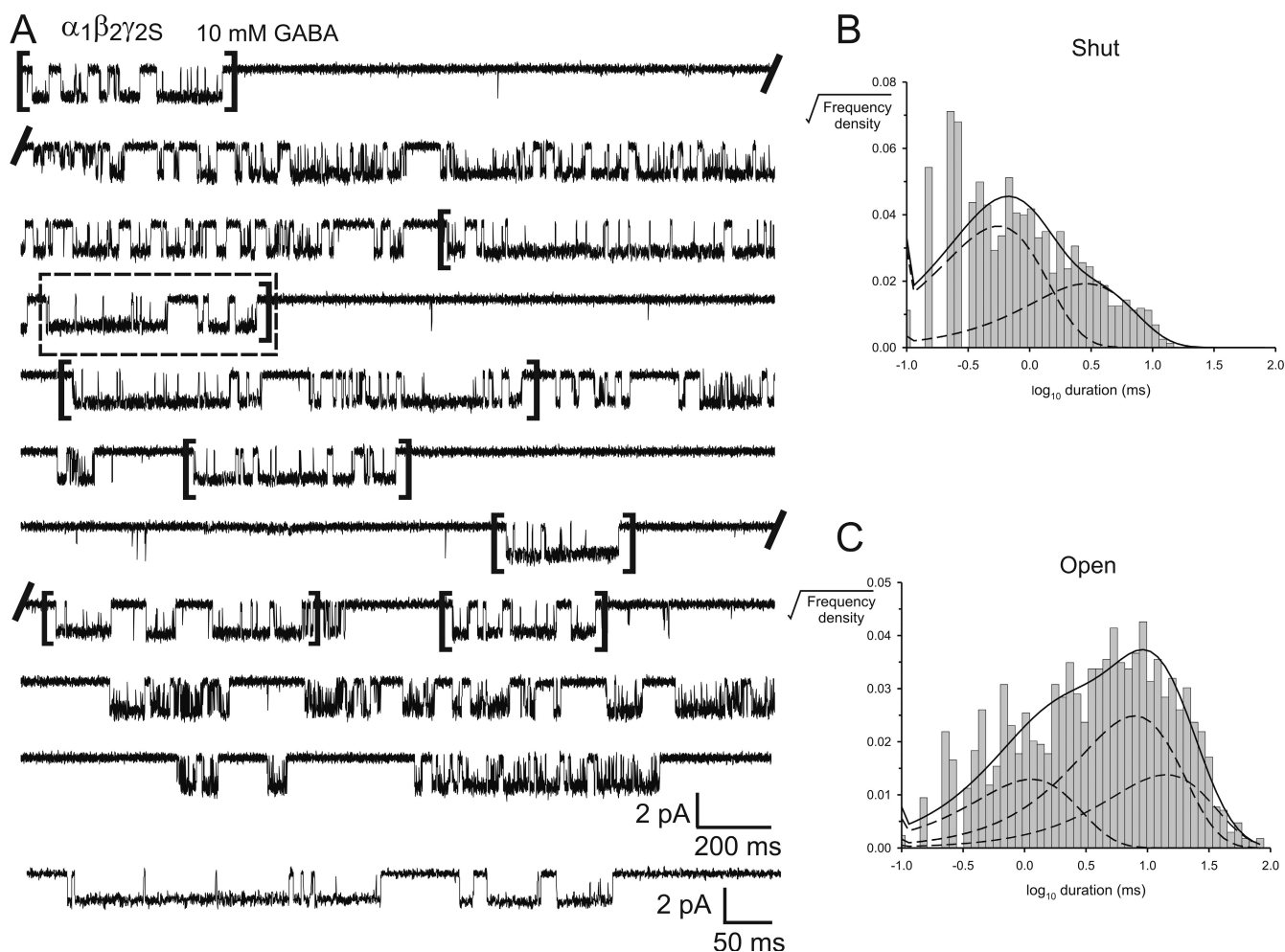
Figure 9. Burst analysis of H-Mode activity in $\alpha_1\beta_2\gamma_{2S}$ GABA$_A$Rs. (A) Continuous, 2-s sweeps of single channel activity recorded from a patch expressing $\alpha_1\beta_2\gamma_{2S}$ GABA$_A$R in response to 10 mM GABA. The break in the recording represents $\sim$0.5–2 min of no activity (desensitization). Clusters of H-Mode activity are enclosed by parentheses. The segment enclosed in the box is expanded below. (B) Dwell time histogram of apparent shut intervals and (C) dwell time histogram of apparent open intervals for the activity shown in A. Distributions were fit with a mixture of exponential probability density functions (dark lines). The individual components are shown as broken lines. The analysis revealed two shut and three open components for this activity. Currents were filtered to 2 kHz for display purposes.

ligation give rise to slightly different open pore conformations, resulting in correspondingly different resistances to ion flow. Our limitation at developing this hypothesis further, however, stems from not knowing the state of ligation of the channels in the presence of high compared with low concentrations of THIP, and indeed, between THIP and GABA. Throughout the study we have assumed that two THIP molecules bind in the same locations as GABA, but we cannot rule out the possibility that THIP may also bind to a site(s) other than the conventionally accepted GABA binding pockets. We can suggest that exposing the channels to saturating concentrations of THIP (5 or 10 mM) may produce a higher degree of ligation than 100 μM THIP. At least two reasonable binding scenarios can be put forward that are consistent with the data. It could be that the activity seen with 100 μM THIP represents monoliganded openings, whereas openings with 5 or 10 mM THIP represent diliganded

openings. Alternatively, both putative "GABA" binding sites may be occupied in the presence of 100 μM THIP and 5 or 10 mM THIP results in additional sites being occupied. Assuming that the channels require two GABA molecules for gating open, these additional sites are likely of low affinity and unavailable to GABA, as the same observation was not made with high GABA concentrations. Candidate sites are the α_1–γ_{2S} or α_4–δ interfaces, but could also be elsewhere. Regardless of the limitations in interpretation we can infer that high concentrations of THIP give rise to open states with subtly different permeation pathways, with respect to geometry and/or the orientation of residues lining the pathway compared with GABA. Consistent with this proposal, a recent study on α_1 homomeric glycine receptors presents compelling data that different glycinergic ligands induce different conformational responses in the pore-lining M2 domains of that channel (Pless et al., 2007). It is also of interest
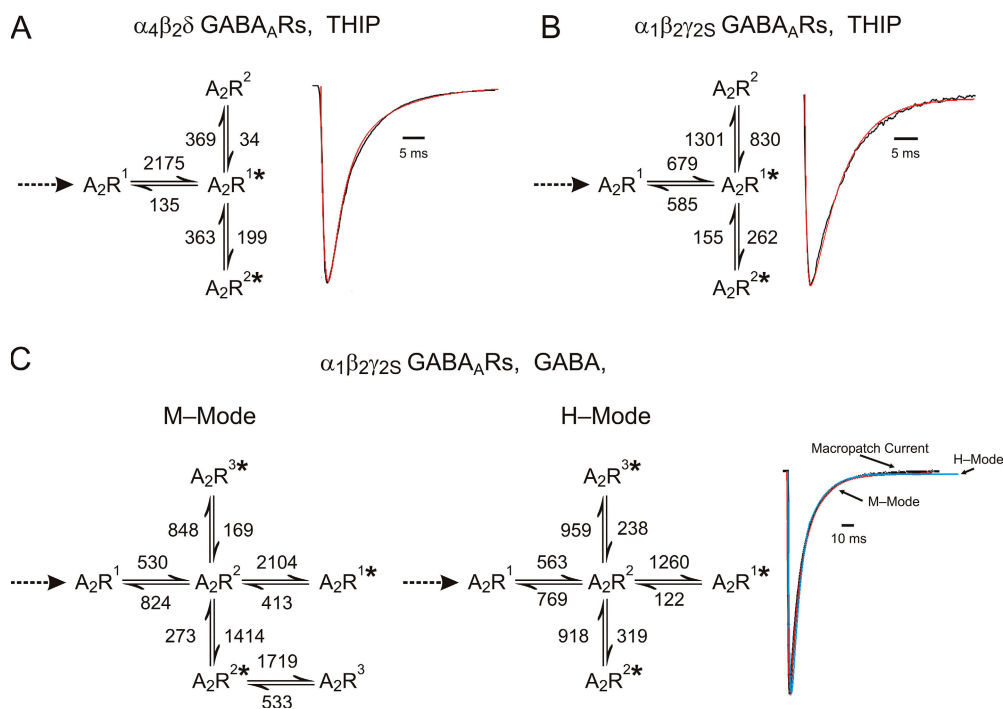
A α4β2δ GABAₐRs, THIP

A_2R^2

369 | 34

2175
A_2R^1 ⇌ A_2R^{1*}
135

363 | 199

A_2R^{2*}

5 ms

B α1β2γ2S GABAₐRs, THIP

A_2R^2

1301 | 830

679
A_2R^1 ⇌ A_2R^{1*}
585

155 | 262

A_2R^{2*}

5 ms

C α1β2γ2S GABAₐRs, GABA,

M–Mode

A_2R^{3*}

848 | 169

530   2104
A_2R^1 ⇌ A_2R^2 ⇌ A_2R^{1*}
824   413

273 | 1414

1719
A_2R^{2*} ⇌ A_2R^3
533

H–Mode

A_2R^{3*}

959 | 238

563   1260
A_2R^1 ⇌ A_2R^2 ⇌ A_2R^{1*}
769   122

918 | 319

A_2R^{2*}

Macropatch Current — H–Mode

M–Mode

10 ms

Figure 10. Kinetic schemes from burst analysis. Kinetic schemes describing activation of α4β2δ GABAₐRs (A) and α1β2γ2S GABAₐRs (B) by 10 mM THIP. The main differences between the two schemes is the opening rate constants leading to A_2R^{1*}. Accompanying each scheme is a current simulation, generated using the scheme with binding steps attached, superimposed on a real macropatch current. (C) Kinetic schemes describing activation of α1β2γ2S GABAₐRs by 10 mM GABA for M-Mode activity (left) and H-Mode activity (right). Note that both modes have a common route to A_2R^{1*} (A_2R^1–A_2R^2–A_2R^{1*}). On the far right are current simulations using the schemes with binding steps included (see Fig. 4), superimposed on a macropatch current.

to contrast the above postulated agonist-specific open states with the existence of multiple open states in the presence of the same agonist, which are all of the same conductance (amplitude) and distinguishable on the basis of open dwell times. It should be noted that our observation that THIP elicits larger single channel openings than GABA is contrary to that reported in a previous study on heterologously expressed α1β2γ2S GABAₐRs. Mortensen et al. (2004) report comparable conductance values for a range of agonists, including GABA and THIP, both of which elicited a conductance of ∼27 pS at −70 mV. We have no explanation for the discrepancy between our result and theirs, except to note that the highest THIP concentration Mortensen et al. used was 3 mM and there seemed to be slight trend toward higher current amplitudes going from low efficacy agonists, like 4-PIOL, to higher efficacy agonist, such as GABA in that study. Agonist-specific conductance, although apparently novel in Cys-loop LGICs, is not unprecedented. Previous studies on AMPA receptors have shown that AMPA elicits a greater conductance than kainate (Swanson et al., 1997). Follow up studies that could illuminate the mechanism by which THIP induces a high conductance could include binding pocket mutagenesis studies, including mutations to equivalent binding pocket positions at α1–γ2S or α4–δ interfaces.

Macropatch Activation, Current Simulations, and Simple Kinetic Schemes

Our ultrafast agonist application experiments produced plots of activation rate over a wide range of agonist

concentrations. From these plots we extracted some informative kinetic parameters, some of which we interpreted within the framework of Scheme 1. First, we determined that THIP activated α4β2δ GABAₐRs with a greater opening rate constant (β) than GABA, but the converse was true at α1β2γ2S GABAₐRs. Second, for α1β2γ2S GABAₐRs, the fitted data produced similar EC50s for activation (k_{obs} EC50), suggesting that THIP and GABA have the same apparent affinity for these channels, with the possible exception of the above-postulated low affinity site(s) for THIP. For α4β2δ GABAₐRs, the small current amplitudes elicited by GABA concentrations <10 mM, partly owing to low channel expression levels, prohibited us from obtaining data for a full k_{obs} plot. The situation was better for THIP at α4β2δ GABAₐRs. That plot produced a k_{obs} EC50 of 1.64 mM suggesting a low apparent affinity for THIP. Finally, we observed that as both agonist concentrations decreased toward zero, the activation plots plateaued, and in the case for α1β2γ2S GABAₐRs, converged to the same lower asymptotic value. The reciprocal of the lower asymptotic value provides an estimate of the minimum burst duration (Maconochie et al., 1994; Colquhoun and Hawkes, 1995) for each experimental circumstance. The estimated minimum burst duration for both agonists at α1β2γ2S GABAₐRs was ∼5 ms. These results indicate that the lower threshold of activation is independent of agonist type for α1β2γ2S GABAₐRs. At α4β2δ GABAₐRs activated by THIP, the minimum bursts duration was ∼2–3 ms, and we suspect that this may also be the case for GABA-activated bursts at these GABAₐRs. In α1β2γ2S GABAₐRs, it has been demonstrated

that mutating a residue that impairs the gating transduction pathway, α_1K220A, also produced a higher k_{obs} minimum asymptote than the wild-type channel, suggesting that the minimum burst duration was decreased by the mutation (Keramidas et al., 2006).

For the purpose of calculating the shutting rate constant (α), and the association (k_{+1}) and dissociation (k_{-1}) rate constants in Scheme 1, we simulated our macropatch currents in response to 1–2-ms exposure to agonist. The opening rate constant and the equilibrium dissociation constant ($K_d = k_{-1}/k_{+1}$) were fixed to the values obtained from the k_{obs} plots (after correction), while α and the individual binding rate constants were allowed to vary during the fitting. The agonist binding rate constants that we obtained facilitated estimates of apparent affinity, as indicated by the equilibrium dissociation constant (affinity = $1/K_d$), of each agonist at each of the two GABA$_A$Rs. For $\alpha_4\beta\delta$ GABA$_A$Rs, the K_d for THIP derived from the plot of activation was 683 μM. From our simulations we predicted a K_d value for GABA of 314 μM, but this value should be viewed with some caution as we were unable to verify it experimentally. At $\alpha_1\beta_2\gamma_{2S}$ GABA$_A$Rs, both agonists had the same apparent affinity ($K_d \sim 290$ μM). Mortensen et al. (2004) also examined the kinetics of $\alpha_1\beta_2\gamma_{2S}$ GABA$_A$Rs, in the context of a similar reaction scheme using GABA and THIP. That study reports equilibrium dissociation constants of $\sim$134 and $\sim$803 μM for GABA and THIP, respectively (a sixfold difference). In contrast, our data lead us to infer that the apparent affinity for both agonists is comparable, and that the main difference between the two agonists is the opening rate constant, with which they activate channels. In the closely related $\alpha_1\beta_1\gamma_{2S}$ GABA$_A$Rs, Lema and Auerbach (2006) derived K_ds for GABA that ranged between 55 and 132 μM, depending on the kinetic scheme used to fit the data, which are between approximately five- and threefold lower than ours. It should also be noted that Scheme 1 does not explicitly postulate any "preconducting" states that represent transitions (intermediate nonconducting states) between agonist binding and opening of the channel. The existence of such states has been proposed for the heteromeric glycine receptor (Burzomato et al., 2004) and the $\alpha_1\beta_1\gamma_{2S}$ GABA$_A$R (Lema and Auerbach, 2006). Here we interpret our affinity calculations as applying to the resting state of the channels, as is inherent in Scheme 1, but cannot rule out the possibility that they may more closely reflect the affinity for some "preconducting" states (Colquhoun, 2007).

Kinetic Properties Revealed by Single Channel Recordings

An analysis of single channel currents revealed that a saturating concentration of THIP elicited similar currents in both channel types. In particular, burst duration was similar; being $\sim$32–33 ms in both channels, and intraburst P_O was also of the same order at $\sim$0.4–0.5 ($P > 0.05$). At a saturating concentration of GABA,

GABA-gated burst duration was, however, dissimilar between the two channels; being in the order of 100 ms at $\alpha_1\beta_1\gamma_{2S}$ channels and <10 ms at $\alpha_4\beta_2\delta$ channels. Our k_{obs} plots suggest that at the threshold of activation, the minimum burst duration is agonist independent, as is evident for $\alpha_1\beta_1\gamma_{2S}$ channels.

We also distinguished at least two (and up to three) bursting patterns, or modes, for $\alpha_1\beta_2\gamma_{2S}$ GABA$_A$Rs in the presence of 10 mM GABA. The most prevalent mode had an intraburst P_O of $\sim$0.7, but in several patches we observed bursts (and clusters) with a higher P_O ($\sim$0.9). These are similar to those reported for $\alpha_1\beta_1\gamma_{2S}$ GABA$_A$Rs in response to 5 mM GABA (Lema and Auerbach, 2006). The mean time constants, τ_{C1}, τ_{C3}, and τ_{O1} for M- and H-Mode activity were comparable. The main difference between the two modes was the second (τ_{O2}) and especially the third (τ_{O3}) open time constants, with τ_{O3} being substantially greater in H-Mode activity. In addition, we occasionally noticed channels gating to an apparently low intraburst P_O (L-Mode, $P_O \sim 0.4$), but this was seen in only 2 of 14 patches.

The origin of modal bursts is unknown, but this type of behavior has been reported in NMDA receptors (Popescu and Auerbach, 2004; Popescu et al., 2004), GABA$_A$Rs (Lema and Auerbach, 2006), glycine receptors (Plested et al., 2007), and acetylcholine receptors (Auerbach and Lingle, 1986; Milone et al., 1998). For all of the above investigations of LGICs, single channel recordings were done in the cell-attached configuration. This might seem to implicate intracellular modulators of channel activity in modal gating. However, modes were seen in excised patches in our experiments, including modal switching within the same cluster of activity (see Fig. 5 A).

A notable feature of channel activation by THIP was that both channels opened directly from the first shut state (A_2R^1). This contrasts with GABA-gated activation of $\alpha_1\beta_2\gamma_{2S}$ GABA$_A$Rs, which entered a second shut state (A_2R^2) before opening, for both M-Mode and H-Mode bursts. Similar schemes were derived by Lema and Auerbach (2006) for $\alpha_1\beta_1\gamma_{2S}$ GABA$_A$Rs and analogous schemes by Burzomato et al. (2004) for $\alpha_1\beta$ glycine receptors; the latter group referring to A_2R^2-like states as "flip" (preconducting) states. Preconducting shut states were notably absent in THIP-gated activity in the present study. It is tempting to speculate that THIP and GABA have access to different gating transduction pathways that culminate in an open pore with different resistances to ion flow.

We also calculated efficacy ($E = \beta/\alpha$) for the transition to A_2R^{1*} from the diliganded state leading to it, A_2R^1 for THIP-gated activity at both channels or A_2R^2 for GABA-gated activity at $\alpha_1\beta_2\gamma_{2S}$ channels. THIP activated $\alpha_4\beta_2\delta$ channels with an efficacy of $\sim$16, whereas at $\alpha_1\beta_2\gamma_{2S}$ channels, THIP was much less efficacious ($E \sim 1.2$). The efficacy with which GABA activated M-Mode and H-Mode activity was $\sim$5.2 and $\sim$10.3, respectively.

## Reconciling Simple and Complex Kinetic Schemes

In the present study we used two different recording techniques; each one records current from channels that are under different experimental conditions. One of these techniques was the rapid application of agonist to macropatches. In this circumstance, the channels are not in equilibrium with agonist and it is assumed that the channels are initially in the unbound shut state (R in Scheme 1), which must first enter the singly bound then doubly bound states before opening. One the other hand, single channel recordings were done in steady-state (equilibrium) conditions, where the shut state(s) that precedes channel bursts are diliganded. For both channels and both agonists, multiple diliganded shut states were incorporated in the complex schemes, compared with only one diliganded shut state for the simple, macropatch-derived schemes. Channel opening must start and end with A_2R for the simple schemes. This is manifestly not the case for complex schemes with multiple diliganded shut states. Taking M-Mode activity as an example, channel opening can arise directly from A_2R^2 or A_2R^3, or any long-lived, diliganded shut ("desensitized") states that could potentially be connected to an open state (e.g., A_2R^3*). We omitted long, nonconducting segments from our single channel analysis and deliberately applied agonist pulses for ~ 1 ms so as to minimize the impact of "desensitization" on our macropatch currents. It is not possible to determine which of these candidate shut states any given burst arises from by inspecting the single channel record, and we have no information about the mean lifetimes of these states. Since the distribution of first latency before channel opening is conditional on the starting state (Colquhoun and Hawkes, 1995), it is unlikely that the macroscopic current can be reproduced by simply averaging aligned single channels bursts (Edmonds and Colquhoun, 1992).

Given these caveats, we opted to select complex schemes on the condition that they were also able to adequately approximate macropatch currents. This amenability strongly suggests that the first latencies before channel opening, for the open states in the complex schemes shown in Fig. 10, are very short (Colquhoun and Hawkes, 1995). In addition, the reasonable reproduction of macropatch activation using complex schemes suggests a single predominant pathway, although this does not imply that the pathways induced by GABA and THIP have to be identical.

There are a number of features of macropatch currents that suggest a simple underlying scheme, with a single dominant activation pathway. These include the single exponential required to fit the onset phase of the current, over the concentration range, and the finite upper and lower limits (asymptotes) for the rate of current development. Activation complexity is suggested by the multiple open and shut exponential components required to fit single channel data and the multiple (usually two) exponentials needed to describe macropatch desensitization and deactivation. One way to reconcile the apparent paradox between simple and complex schemes is to postulate two groups of states, on either side of a principal activation pathway. One group, referred to as inactive, consists of unliganded and suboptimally liganded states, such as AR in Scheme 1, and brief open states that account for a negligible percentage of the macroscopic current. The other group, termed active, contains fully liganded open and shut states that are not negligibly brief (orders of magnitude slower than binding). The rate constants that govern the transitions between the inactive and active collections of states describe the principal activation pathway, as illustrated in Scheme 2 (Maconochie et al., 1994).

<div align="right">(SCHEME 2)</div>
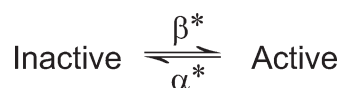
$$\text{Inactive} \underset{\alpha^*}{\overset{\beta^*}{\rightleftharpoons}} \text{Active}$$

The k_{obs} over the entire concentration range is described by the sum of rates going from the inactive to active states (β^*) and rates going from the active to inactive states (α^*). At low agonist concentrations, the channels are rarely fully liganded and the reaction favors the inactive group of states. Under this circumstance, β^* approaches zero and the duration that the channels exist in the active group is $1/\alpha^*$, otherwise referred to as the low concentration burst duration. At the other extreme, where agonist concentration is saturating, full ligation is prevalent and the activation pathway favors channels moving into the active group of states. Here, the rate of exiting the inactive collection of states will approach the opening rate constant for the predominant open state, after subtraction of α^*, assuming that there are no fully liganded channels that enter long-lived shut states within the inactive group (Maconochie et al., 1994; Colquhoun and Hawkes, 1995).

Conclusion

In summary, we have recorded ensemble and single channel activity, using GABA and THIP, from two different forms of recombinant GABA$_A$Rs, one reflecting the typical subunit composition of synaptic GABA$_A$Rs, and the other corresponding to a major subtype of extrasynaptic GABA$_A$Rs. Saturating concentrations of THIP elicited 35–37-pS openings in both channel types, whereas GABA and subsaturating concentrations of THIP elicited ~ 25-pS openings in both channel types, suggesting that the degree of channel ligation influences the conducting state of the channels. The $\alpha_1\beta_2\gamma_{2S}$ (synaptic-type) GABA$_A$Rs were characterized by bursts of openings in response to saturating concentrations of GABA and revealed up to three distinct modes of gating, each mode characterized by stable periods of open probability. The predominant M and H Modes both featured long bursts

of channel openings. In contrast, the $\alpha_4\beta_2\delta$ (extrasynaptic-type) and $\alpha_1\beta_2\gamma_{2S}$ GABA$_A$Rs showed only a single gating mode in the presence of THIP, with a preponderance of brief channel openings and infrequent bursts of moderate duration. The biophysical properties of these receptors are well suited to their physiological functions; $\alpha_1\beta_2\gamma_{2S}$ channels open with high probability when saturated by neurotransmitter. $\alpha_4\beta_2\delta$ channels open with low probability, even when activated by saturating transmitter levels.

REFERENCES

Akk, G., J. Bracamontes, and J.H. Steinbach. 2004. Activation of GABA$_A$ receptors containing the $\alpha 4$ subunit by GABA and pentobarbital. *J. Physiol.* 556:387–399.

Auerbach, A., and C.J. Lingle. 1986. Heterogeneous kinetic properties of acetylcholine receptor channels in *Xenopus* myocytes. *J. Physiol.* 378:119–140.

Barry, P.H. 1994. JPCalc, a software package for calculating liquid junction potential corrections in patch-clamp, intracellular, epithelial and bilayer measurements and for correcting junction potential measurements. *J. Neurosci. Methods.* 51:107–116.

Baumann, S.W., R. Baur, and E. Sigel. 2002. Forced subunit assembly in $\alpha_1\beta_2\gamma_2$ GABA$_A$ receptors. Insight into the absolute arrangement. *J. Biol. Chem.* 277:46020–46025.

Brickley, S.G., S.G. Cull-Candy, and M. Farrant. 1996. Development of a tonic form of synaptic inhibition in rat cerebellar granule cells resulting from persistent activation of GABA$_A$ receptors. *J. Physiol.* 497:753–759.

Brown N., J. Kerby, T.P. Bonnert, P.J. Whiting, and K.A. Wafford. 2002. Pharmacological characterization of a novel cell line expressing human $\alpha_4\beta_3\delta$ GABA$_A$ receptors. *Br. J. Pharmacol.* 136:965–974.

Burzomato, V., M. Beato, P.J. Groot-Kormelink, D. Colquhoun, and L.G. Sivilotti. 2004. Single-channel behavior of heteromeric $\alpha 1\beta$ glycine receptors: an attempt to detect a conformational change before the channel opens. *J. Neurosci.* 24:10924–10940.

Chang, Y., R. Wang, S. Barot, and D.S. Weiss. 1996. Stoichiometry of a recombinant GABA$_A$ receptor. *J. Neurosci.* 16:5415–5424.

Cobb, S.R., E.H. Buhl, K. Halasy, O. Paulsen, and P. Somogyi. 1995. Synchronization of neuronal activity in hippocampus by individual GABAergic interneurons. *Nature.* 378:75–78.

Colquhoun, D. 2007. What have we learned from single ion channels? *J. Physiol.* 581:425–427.

Colquhoun, D., and A.G. Hawkes. 1995. The principles of the stochastic interpretation of ion-channel mechanisms. *In* Single-Channel Recordings. Second edition. Plenum Press, NY. 397–482.

Darlison, M.G., I. Pahal, and C. Thode. 2005. Consequences of the evolution of the GABA$_A$ receptor gene family. *Cell. Mol. Neurobiol.* 25:607–624.

Del Castillo, J., and B. Katz. 1957. Interaction at end-plate receptors between different choline derivatives. *Proc. R. Soc. Lond. B. Biol. Sci.* 146:369–381.

Edmonds, B., and D. Colquhoun. 1992. Rapid decay of averaged single-channel NMDA receptor activations recorded at low agonist concentration. *Proc. R. Soc. Lond. B.* 250:279–286.

Gingrich, K.J., W.A. Roberts, and R.S. Kass. 1995. Dependence of the GABA$_A$ receptor gating kinetics on the α-subunit isoform: implications for structure-function relations and synaptic transmission. *J. Physiol.* 489:529–543.

Hamill, O.P., A. Marty, E. Neher, B. Sakmann, and F.J. Sigworth. 1981. Improved patch-clamp techniques for high-resolution current recording from cells and cell-free membrane patches. *Pflugers Arch.* 391:85–100.

Hardie, J.B., and R.A. Pearce. 2006. Active and passive membrane properties and intrinsic kinetics shape synaptic inhibition in hippocampal CA1 pyramidal neurons. *J. Neurosci.* 26:8559–8569.

Jia, F., L. Pignataro, C.M. Schofield, M. Yue, N.L. Harrison, and P.A. Goldstein. 2005. An extrasynaptic GABA$_A$ receptor mediates tonic inhibition in thalamic VB neurons. *J. Neurophysiol.* 94:4491–4501.

Jia, F., M. Yue, D. Chandra, A. Keramidas, G.E. Homanics, P.A. Goldstein, and N.L. Harrison. 2008. Taurine is a potent activator of extrasynaptic GABA$_A$ receptors in the thalamus. *J. Neurosci.* 28(1):106–115.

Jones, M.V., and G.L. Westbrook. 1995. Desensitized states prolong GABA$_A$ channel responses to brief agonist pulses. *Neuron.* 15:181–191.

Keramidas, A., A.J. Moorhouse, K.D. Pierce, P.R. Schofield, and P.H. Barry. 2002. Cation-selective mutations in the M2 domain of the inhibitory glycine receptor channel reveal determinants of ion-charge selectivity. *J. Gen. Physiol.* 119:393–410.

Keramidas, A., T.L. Kash, and N.L. Harrison. 2006. The pre-M1 segment of the α_1 subunit is a transduction element in the activation of the GABA$_A$ receptor. *J. Physiol.* 575:11–22.

Knoflach, F., D. Benke, Y. Wang, L. Scheurer, H. Luddens, B.J. Hamilton, D.B. Carter, H. Mohler, and J.A. Benson. 1996. Pharmacological modulation of the diazepam-insensitive recombinant γ-aminobutyric acid$_A$ receptors $\alpha 4\beta 2\gamma 2$ and $\alpha 6\beta 2\gamma 2$. *Mol. Pharmacol.* 50:1253–1261.

Lavoie, A.M., J.J. Tingey, N.L. Harrison, D.B. Pritchett, and R.E. Twyman. 1997. Activation and deactivation rates of recombinant GABA$_A$ receptor channels are dependent on α-subunit isoform. *Biophys. J.* 73:2518–2526.

Lema, G.M., and A. Auerbach. 2006. Modes and models of GABA$_A$ receptor gating. *J. Physiol.* 572:183–200.

Li, P., D.F. Covey, J.H. Steinbach, and G. Akk. 2006. Dual potentiating and inhibitory actions of a benz[e]indene neurosteroid analog on recombinant $\alpha 1\beta 2\gamma 2$ GABA$_A$ receptors. *Mol. Pharmacol.* 69:2015–2026.

Maconochie, D.J., and J.H. Steinbach. 1998. The channel opening rate of adult- and fetal-type mouse muscle nicotinic receptors activated by acetylcholine. *J. Physiol.* 506:53–72.

Maconochie, D.J., J.M. Zempel, and J.H. Steinbach. 1994. How quickly can GABA$_A$ receptors open? *Neuron.* 12:61–71.

McKernan, R.M., and P.J. Whiting. 1996. Which GABA$_A$-receptor subtypes really occur in the brain? *Trends Neurosci.* 19:139–143.

Milone, M., H.L. Wang, K. Ohno, R. Prince, T. Fukudome, X.M. Shen, J.M. Brengman, R.C. Griggs, S.M. Sine, and A.G. Engel. 1998. Mode switching kinetics produced by a naturally occurring mutation in the cytoplasmic loop of the human acetylcholine receptor epsilon subunit. *Neuron.* 20:575–588.

Mody, I. 2001. Distinguishing between GABA$_A$ receptors responsible for tonic and phasic conductances. *Neurochem. Res.* 26:907–913.

Mortensen, M., U. Kristiansen, B. Ebert, B. Frolund, P. Krogsgaard-Larsen, and T.G. Smart. 2004. Activation of single heteromeric GABA$_A$ receptor ion channels by full and partial agonists. *J. Physiol.* 557:389–413.

Nusser, Z., N. Hajos, P. Somogyi, and I. Mody. 1998. Increased number of synaptic GABA$_A$ receptors underlies potentiation at hippocampal inhibitory synapses. *Nature.* 395:172–177.

Pless, S.A., M.I. Dibas, H.A. Lester, and J.W. Lynch. 2007. Conformational variability of the glycine receptor M2 domain

in response to activation by different agonists. *J. Biol. Chem.* 282:36057–36067.

Plested, A.J., P.J. Groot-Kormelink, D. Colquhoun, and L.G. Sivilotti. 2007. Single-channel study of the spasmodic mutation α1A52S in recombinant rat glycine receptors. *J. Physiol.* 581:51–73.

Popescu, G., and A. Auerbach. 2004. The NMDA receptor gating machine: lessons from single channels. *Neuroscientist.* 10:192–198.

Popescu, G., A. Robert, J.R. Howe, and A. Auerbach. 2004. Reaction mechanism determines NMDA receptor response to repetitive stimulation. *Nature.* 430:790–793.

Purohit, Y., and C. Grosman. 2006. Estimating binding affinities of the nicotinic receptor for low-efficacy ligands using mixtures of agonists and two-dimensional concentration-response relationships. *J. Gen. Physiol.* 127:719–735.

Schofield, C.M., and J.R. Huguenard. 2007. GABA affinity shapes IPSCs in thalamic nuclei. *J. Neurosci.* 27:7954–7962.

Sieghart, W., and G. Sperk. 2002. Subunit composition, distribution and function of GABA$_A$ receptor subtypes. *Curr. Top. Med. Chem.* 2:795–816.

Sigel, E., R. Baur, N. Boulineau, and F. Minier. 2006. Impact of subunit positioning on GABA$_A$ receptor function. *Biochem. Soc. Trans.* 34:868–871.

Somogyi, P., J.M. Fritschy, D. Benke, J.D. Roberts, and W. Sieghart. 1996. The γ2 subunit of the GABA$_A$ receptor is concentrated in synaptic junctions containing the α1 and β2/3 subunits in hippocampus, cerebellum and globus pallidus. *Neuropharmacology.* 35:1425–1444.

Steinbach, J.H., and G. Akk. 2001. Modulation of GABA$_A$ receptor channel gating by pentobarbital. *J. Physiol.* 537:715–733.

Sur, C., S.J. Farrar, J. Kerby, P.J. Whiting, J.R. Atack, and R.M. McKernan. 1999. Preferential coassembly of α4 and δ subunits of the γ-aminobutyric acid$_A$ receptor in rat thalamus. *Mol. Pharmacol.* 56:110–115.

Swanson, G.T., S.K. Kamboj, and S.G. Cull-Candy. 1997. Single-channel properties of recombinant AMPA receptors depend on RNA editing, splice variation, and subunit composition. *J. Neurosci.* 17:58–69.

Vicini, S., C. Ferguson, K. Prybylowski, J. Kralic, A.L. Morrow, and G.E. Homanics. 2001. GABA$_A$ receptor α1 subunit deletion prevents developmental changes of inhibitory synaptic currents in cerebellar neurons. *J. Neurosci.* 21:3009–3016.

Wagner, D.A., C. Czajkowski, and M.V. Jones. 2004. An arginine involved in GABA binding and unbinding but not gating of the GABA$_A$ receptor. *J. Neurosci.* 24:2733–2741.

Whittemore, E.R., W. Yang, J.A. Drewe, and R.M. Woodward. 1996. Pharmacology of the human γ-aminobutyric acid$_A$ receptor α4 subunit expressed in *Xenopus laevis* oocytes. *Mol. Pharmacol.* 50:1364–1375.